A NUMERICAL STUDY OF TILLAGE TOOL WEAR DURING PLOWING OF SANDY SOIL

by

Gaurav S. Goel

A dissertation submitted to the faculty of the
University of North Carolina at Charlotte in
partial fulfillment of the requirements
for the degree of Doctor of Philosophy in
Mechanical Engineering

Charlotte

2013

Approved by:

_____
Dr. Harish P. Cherukuri

_____
Dr. Ronald E. Smelser

_____
Dr. David C. Weggel

_____
Dr. Yogendra P. Kakad

ABSTRACT

GAURAV S. GOEL. A numerical study of tillage tool wear during plowing of sandy soil. (Under the direction of DR. HARISH P. CHERUKURI)

Wear of tillage tools during tilling operations leads to increase in power requirements, frequent downtimes for tool replacement, loss of production and an increase in the equipment and operational costs. A large number of variables - such as the moisture content in the soil, soil particle sizes, plowing speed, plowing depth, tool material properties, etc. - influence the tool wear rates. In turn, the tool wear has an effect on the power requirements for the tilling operations since a worn out tool requires larger amounts of power. The purpose of the present work is to (a). develop finite element models for predicting tool wear and power requirements, (b). validate the finite element models with experiments, and (c). study the effect of the above-mentioned variables on tool wear and power requirements. The ultimate objective is to understand the primary mechanisms behind tool wear and devise new designs for tillage tools to mitigate tool wear rates.

The tool wear process is treated as a two-body abrasion where a rigid sand particle scratches against the surface of the tillage tool at a prescribed speed. A finite element model is developed to model the scratching process. The deformations predicted by the finite element models are used in conjunction with the classical ploughing theory and the material removal factor to identify the mechanisms underlying the wear of the tillage tool. The predicted material removal factors are compared with experimental results and a parametric study is carried out to study the effect of various parameters on tool wear.

A two-dimensional finite element model simulating the soil-tool interaction during tilling is also developed. The purpose of this model is to study the feasibility of using the finite element methods to predict power requirements during a tilling process. The tillage tool is modeled as a rigid body moving through soil at a prescribed speed. The

constitutive behavior of the soil is assumed to be given by the Drucker-Prager model. The forces acting on the tillage tool as the tool moves through soil are calculated and the power required for the tilling operation is calculated using these forces.

The computed values for tool material loss and power consumed during plowing operations are found to be in reasonable agreement with the experimental results. In addition, the parametric studies show that the primary wear mechanism is a combination of ploughing and cutting with cutting being dominant. More sophisticated models and analyses are needed to further understand the tillage tool wear process. The present work provides the foundation on which these advances can be made.

ACKNOWLEDGMENTS

My first and foremost affirmation goes to my advisor, Dr. Harish Cherukuri, for his encouragement, advice, and great interest in the pursuit of my research and in the timely suggestions to write my dissertation. I would like to convey my sincere thanks to the Department of Mechanical Engineering and Engineering Science for their support throughout my studies.

Besides my advisor, Dr. Cherukuri, I would like to express my sincere thanks to my dissertation committee members: Dr. Ron Smelser, Dr. Dave Weggel, and Dr. Yogendra Kakad, on agreeing to serve on my dissertation committee, and encouraging me to work on my research project.

In addition, I would like to acknowledge the Tribology and Surfaces Group, School of Materials Engineering, National University of Colombia, especially Dr. Alejandro Toro, for the support throughout my studies.

My sincere thanks also goes to the faculty in Mechanical Engineering for the teaching assistantships offered from time to time during my course of studies. Additionally, I would like to thank my friends and colleagues for their subsistence support during my stay as a doctoral student.

Also, I would like thank my parents, Prof. H. S. Goel and Prabha Goel, for encouraging me to pursue doctorate studies and supporting me throughout my life. Last but not the least, I would like to praise my wife Ruchi and kid Shubhi for their patience and encouragement that helped me to complete my research successfully.

TABLE OF CONTENTS

LIST OF FIGURES

LIST OF TABLES

CHAPTER 1: INTRODUCTION

Abrasive wear is one of the primary mechanisms by which tillage tools experience material loss during soil tillage. It has been observed that the tool material loss can be as much as 10 gm per kilometer of tilling. The worn tool (Figure 1.1) leads to poorly tilled soil and consequently needs to be replaced. The replacement can be as frequent as two to three days. Such frequent requirements coupled with the fact that the replacement tools may not be readily available leads to frequent downtimes and consequently significant increases in operational costs. The costs can be further higher if the wear is severe enough that the entire plowing assembly needs to be replaced. Tool wear is also associated with the power required to till the soil. As the tool wears, more energy is required to achieve the same tillage quality. This has the effect of increasing the overall cost of tillage operation.

Figure 1.1: A worn-out tillage tool that needs replacement, Santa F*é* de Antioquia, Colombia.

Sand and gravel are the primary constituents of a typical soil that cause wear in tillage tools. During the soil-tool interaction, the tool wear rates and power consumption are also influenced by a number of other operating parameters associated with the tilling operation. The moisture content of the soil has the effect of reducing the shear strength of the soil. The plowing depth, the plowing/tillage speed and the tool properties are also possible factors influencing tool wear. Consequently, it is important to develop a detailed model of soil-tool interaction to understand the effect that these parameters have on tool wear and on the power requirements for tilling.

1.1 Materials and Methods

The tillage process examined here is carried out with a single tillage tool (also termed a chisel) attached to a plowing assembly. The complete assembly plows the soil at a constant depth of 300 mm from the surface of the soil. This process involves a tractor carrying three individual plowing assemblies that travel at an average linear speed of 3-5 km/hr (Figure 1.2).

Figure 1.2: An arrangement of three plowing assemblies attached to a tractor used for soil tillage.

Soil tillage is a complex tribological phenomenon that involves friction and wear with negligible lubrication. The plowing assembly carrying a tillage tool is moved

horizontally at a constant (tillage) speed with a prescribed depth (also called the plowing depth). Figure 1.3 shows this. The tool movement causes shear failure in the soil. This results in the soil breaking into smaller aggregates along the tool surfaces. The broken soil particles slide along the tool surfaces. The various soil particles induce tool surface deformation to differing degrees of intensity with some causing large enough stresses and deformation to cause material separation at the tool surface and thus resulting in tool wear. Plowing operations and the quality are influenced by a number of factors [44]. These variables can be intrinsic or external to the system, and they affect the rate of tool wear during tilling operations [40, 59, 70].

Figure 1.3: Plowing operation in a silt loam soil, Santa F*é* de Antioquia, Colombia.

In this work, observations are included from field tests conducted by the Tribology and Surfaces Group, School of Materials Engineering, National University of Colombia-Medellin. These tests were carried out to investigate the effect of various parameters, such as plowing depth, soil resistance to penetration, soil moisture content and tillage speed on the tool life. Similar studies from both experimental and analytical points of view have been made previously [5,27,29,44,54]. The observations from the field tests carried out in Colombia are outlined in the following sections.

1.1.1 Tillage Tool Material

Figure 1.4 shows a schematic of a tillage tool attached to a plowing assembly. The tillage tool is made from heat-treated alloy steel. The purpose of heat-treating the tool material is to improve its hardness and to lower tool wear. The tillage tools used in the field tests conducted in Colombia were made of heat-treated DIN 30MnB5 alloy steel.

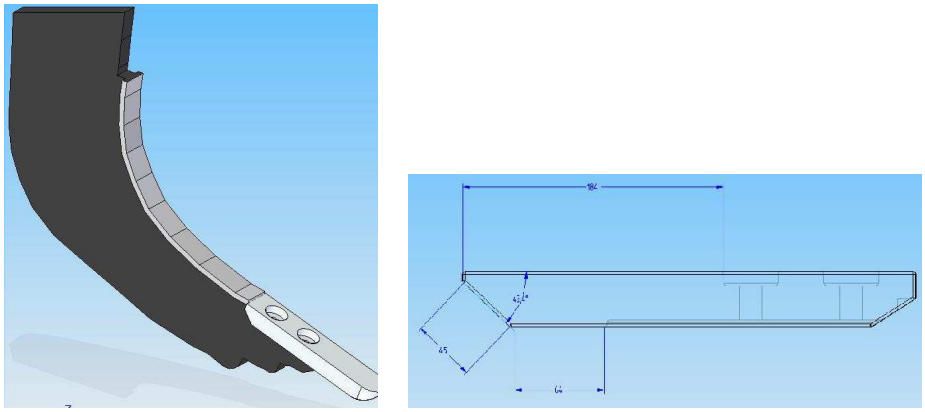

(a) (b)

Figure 1.4: (a). The plowing assembly and (b). A 2D schematic of a tillage tool.

The tests were conducted with a tillage tool whose dimensions are 6 cm in width and 12 cm in length. An unworn tool and a worn tool are shown in Figure 1.5. The worn tool is shown along with the unworn tool to highlight the severity of wear that is experienced in tilling operations. Clearly, the worn tool, if not replaced, compromises the tillage quality. The tool wear is measured by the amount of lost material. This amount is estimated by measuring the difference in the weight of a tool before and after the tillage process (Figure 1.6) [61].

1.1.2 Soil Material

A typical soil is made of silt, clay, sand, and gravel. The silt and clay are smaller-sized soil particles (less than 0.05 mm), while sand (0.05 mm to 2.0 mm) and gravel (greater than 2 mm) are larger particles. It is an established fact that sand and

(a) (b)

Figure 1.5: A comparison of an unworn tillage tool with a worn tillage tool, (a). top view, and (b). side view.

Figure 1.6: Tool material loss is measured as the difference in the weights of a tillage tool before and after the soil tillage.

gravel account for maximum tool wear. This observation is in congruence with the previous experimental studies that have been conducted to understand tool wear in soil plowing [66].

In addition to several factors like tillage tool material, tool shape, plowing depth, and speed of plowing that affect the tool wear and the power consumption, the type of soil that is tiled, its composition, moisture content and density of soil at site do

Figure 1.7: A view of a field on completion of a tillage process in Colombia.

influence the performance of a tool (material) and its wear and tear. Soils that are more frictional in nature due to the high percentage of coarse grained granular material like sand present are very abrasive in nature and result in abnormal tool wear. Main mineralogical composition sand is Quartz. Quartz is one of the hardest substances known, whose hardness value is much higher than most metallic materials [3,69]. The angle of incidence (impact) on the tillage tool contributes significantly to the magnitude of abrasion of the tool [66,67].

The virgin soil and tool interaction is further complicated if once the field is cultivated. The residual roots left behind after the harvest makes the soil matrix at site as a composite material of soil and residual roots. The study on soil-tool interaction now gets more complex as it is hard to predict the amount of resistance and resulting tool wear in such a field condition. Previous works reported indicate that it is impractical to carry out an exhaustive experimental study on the tool wear due to the limited availability of field data [64]. Some of these properties depend on the geological location of the fields, nature of soils, and crop history of the fields [21,61].

Therefore, to understand the tool wear it is necessary to develop appropriate

constitutive models to portray the material (soil) characteristics and stress-strain behavior, to apply in the numerical (finite element) studies. However, in the absence of such constitutive models, the field studies and the data available from the literature provide motivation for a realistic approach to understand the abrasive wear of tillage tool and its life to use [31,65]. In this study, field data provided is used in the analysis for a complete understanding of tool wear occurring during plowing operations.

1.2 Dissertation Organization

The rest of the dissertation is organized as follows.

In Chapter 2, a literature review is presented, which highlights the observations from the wear related studies conducted by various scientists. These observations primarily focus on the mechanisms that govern the tool surface failure . Additionally, the review also focuses on the various attempts that have been made to predict the wear of metals using finite element studies. Further, this chapter features the conclusions made by researchers who conducted experimental studies to understand the tool wear and the effects of how the tool wear rates are affected by the process variables during tilling operations.

Chapter 3 discusses ABAQUS/Explicit software which is used to conduct simulations of soil-tool interaction and the wear process. This part of the study highlights the important features of the software that are relevant to the problem under consideration in this work. The explicit algorithm, the adaptive meshing technique to refine the mesh dynamically in the regions of high deformations and the contact algorithms used are discussed.

Chapter 4 presents a detailed description of the wear related studies that have been made to estimate the tool wear loss. This includes a discussion of the observations made from the field tests, followed by the assumptions required to create the model. This section covers the preprocessing stage of the finite element models and involves the model geometry, analysis steps, contact, and meshing. Also, included in

this chapter are results from the simulations that were run to estimate the tool wear losses. Conclusions for the numerical predictions made to estimate the material loss from the tool surfaces are included.

Chapter 5 describes the numerical studies conducted to estimate the power requirements during soil tillage. The second part of this study discusses the steps taken to generate the finite element model and the simulation results for the soil deformation due to movement of the plowing assembly. Also, this chapter includes conclusions from the parametric studies conducted to understand the dependence of the power needed for tilling operations on various tilling parameters.

Chapter 6 presents conclusions and recommendations for future work.

CHAPTER 2: LITERATURE REVIEW

In this chapter, a review of the published work on tilling operations is presented. The focus will be on only the work that addresses tool wear, power consumption during tilling and the simulations (computational and analytical) of tilling operations.

Tilling operations involve plowing large amounts of soil and consequently, consume large amounts of power. Of the total energy consumed during soil tillage, the major portion of the energy consumption is attributed to the movement of the tool carrying the plowing assembly in the soil [54, 65]. The amount of energy required to till a given volume of soil is influenced by the condition of the tillage tool, i.e., whether the tool is worn or unworn, and soil properties. The volume of the tilled material is equal to the field area times the plowing depth which usually is about 100 mm [54]. The plowing depth and the tillage area affect tool wear and consequently, the power consumed is affected indirectly as well by these two factors.

In the field, tool wear is estimated by measuring the difference in the weights of a tillage tool before and after the soil plowing. In practice, a tillage tool is designed either to cut or to shape the soil. Tool wear during soil cutting is estimated by measuring the weight of a tool before and after the plowing operation; while in the soil shaping, the tool wear loss is determined by measuring the dimensions of a tool before and after the soil tillage. Owsiak found that more severe wear losses are found in soil cutting tool types [23]. Therefore, his work focused on determining the tool wear loss in cutting tools.

As mentioned above, tool wear loss is influenced by the soil conditions, operating factors, and tool material properties. Soil is an nonhomogeneous material that is made of organic and inorganic matter. A large number of factors influence its mechanical

behavior. The constitutive model describing the mechanical behavior of soil must be simple to implement and yet include the most important of these factors for accurate predictions of tool wear rates [23, 54].

Natsis et al. [66] also studied tool wear and wear rates in soil tillage. They concluded from their studies that the rate of tool wear is associated with the hardness of a soil particle, moisture content, plowing conditions, and hardness of a tool material. They found that an increase in the soil moisture content reduces tool wear, but the tool wear rates increase when the soil type is sandy. Also, a higher wear rate is observed with an increase in the plowing area.

Horvat et al. [65] found that the modification of a soil structure consumes major portion of the energy applied during plowing operations. They found that the power consumption and tool wear are linked with the friction between the soil and tool surface and concluded that the amount of energy consumption is related with the frictional forces existing during the soil-tool interaction. To determine the tool wear, the dimensions of a plowing tool were measured before and after the soil plowing. Their work indicates that the tool wear rates are affected by the soil and tool material properties. They concluded that a comprehensive understanding of tool wear using an experimental approach is not possible due to a number of process parameters and the high costs involved in acquiring the field data.

To overcome the limitations of experimental studies, researchers attempted various analytical and numerical techniques to study tool wear in tilling. The finite element method was the most popular tool used. However, these studies were limited and focused on comparing the tool forces observed during soil plowing. Furthermore, efforts made to study the tool wear using numerical techniques were restricted to a qualitative comparison of the tool forces. The primary reason for this was missing field data. This restricted these studies to an estimate of the tool forces and wear losses could not be calculated.

Generally, tillage tools are made of alloy steel that is heat treated to improve its hardness. Er et al. [56] investigated wear of a plowshare made of a carbide steel hardened by powder boriding and made a comparison of the weights of a virgin and worn plowshare to estimate the wear losses. This technique was then used to understand the effects of the shape of a tillage tool has on the tool wear rates. For a better understanding of tool wear, Owsiak determined tool wear loss based on the measurements of linear wear. This laboratory approach accounts for wear loss when a tillage tool has different shape and different thicknesses of the zone of heat treatment [23]. He found that the wear of soil cutting tools is linearly dependent on the distance traveled by the tool.

2.1 Wear

In the field of tribology, abrasion of a metallic surface has been a topic of research for many years. Furthermore, literature provides a number of references in which wear loss due to abrasion on the metal surface has been determined analytically. Additionally, quite a large amount of work has been done using the finite element method to estimate the wear loss in metals. Abrasive wear of a tillage tool occurs mainly due to the abrasion by the hard soil particles that rub against the tool during tilling and often lead to the material loss from the tool surface. Tillage tools are subjected to material losses primarily due to abrasive wear; this observation is useful in estimating the tool wear losses during soil tilling.

Bayhan [54] claims that agricultural tools wear due to impact, abrasion, fretting, and chemical action. Zum Gahr and other researchers define wear as a tribological phenomenon that results in permanent deformation which gradually leads to material removal from the wearing surface when there is a relative motion between the contacting surfaces [10, 17]. Based on the work done by Zum Gahr, a wear process is categorized into the following major types [10, 58]:

1. Adhesion

2. Surface Fatigue

3. Tribochemical Reaction

4. Abrasion

2.1.1 Adhesive Wear

In adhesive wear, surface failure is the result of the failure of junctions that are formed between the asperities of two contacting surfaces. The junctions are formed between the contacting surfaces that result in a bond formation between the asperities of the two surfaces under high pressure. This leads to permanent deformation between the surfaces in the form of cold welded junctions between the joined surface asperities. With relative sliding of the surfaces, the junctions break and lead to material transfer from one surface to the other (see Figure 2.1).

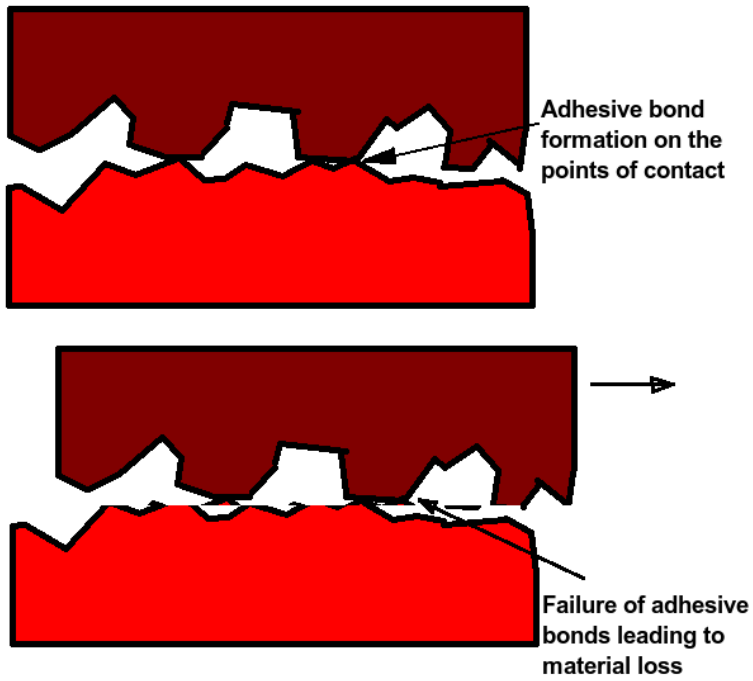

Figure 2.1: Adhesive wear phenomenon.

The amount of material transfer is affected by material properties, overloading, velocity, and temperature of the contacting surfaces. However, the most influential

property is material hardness. An extended form of adhesive wear is a surface seizure; it prevents further motion with an increase in friction coefficient and wear between the surfaces. The adhesive wear between the sliding surfaces continues as long as the shear strength of the cold-weld junctions is less than the material strength. During soil tillage, it has been observed that the larger soil particles separate after indenting and/or scratching the tool surfaces [54].

2.1.2 Surface Fatigue Wear

Surface fatigue is observed with crack formation and propagation. This leads to further material removal in the form of flakes from the solid surface (see Figure 2.2). With repeated cyclic loading, this wear type propagates rapidly. The interaction type between the surfaces can be rolling, sliding, or a combination of both. Sometimes, the impact loading by solids and/or liquid results in fatigue wear. The surface deformation is elasto-plastic and is followed by work hardening and/or work softening, leading to crack formation and propagation. The cracks can be found on the surface, but sometimes they are hidden inside the body.

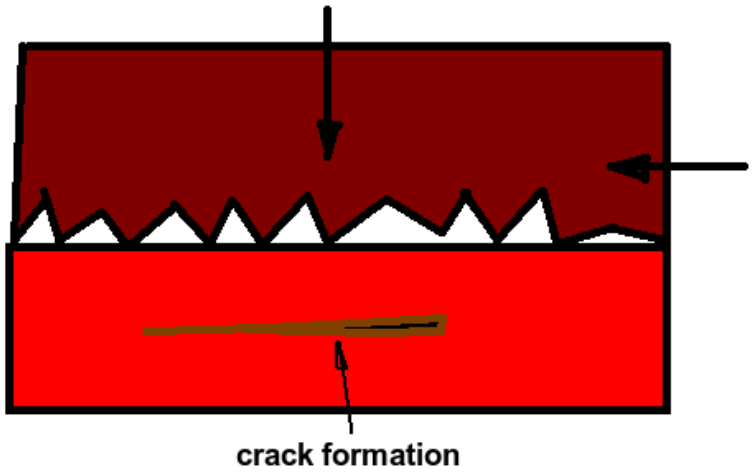

Figure 2.2: Surface fatigue wear that initiates crack formation.

Previous studies have shown that the impinging bodies result in excessive material removal from the wearing surface. This type of deformation is observed when a

tribosystem involves lubrication between the contacting surfaces. This wear mechanism is classified as blast erosion, thermal erosion, cavitation erosion, and other types, depending on the type of environment and the counter-body material. Since soil-tool interaction involves wear and friction in the absence of lubrication, the effects of surface fatigue wear have been ignored in this work. Also, the field tests indicate that the tool surface is rarely subjected to fatigue wear during soil tillage.

2.1.3 Tribochemical Wear

When two rubbing solid surfaces react with a gaseous or liquid environment, material loss occurs with the removal of the surface material and the oxidized material from the surfaces. The continuous occurrence of these reactions result in the propagation of this phenomenon. The tribochemical wear can be due to adhesion between the surface asperities, or the material removed can act as an abrasive agent. Other mechanisms involved in this wear type are the formation or cracking of the oxidized layer which results from the material reaction with the environment. This type of wear phenomenon is rarely observed during soil tillage. The soil deformation is a continuous process in which the soil particles in contact with the tool surface are replaced by the new soil particles in the unplowed soil mass while the plowing assembly is moving forward into the soil.

2.1.4 Abrasive Wear

The abrasive wear phenomenon occurs when the harder surface interacting with the softer surface leads to material removal from the wearing softer surface. The removed material enters the tribosystem and acts as the harder abrasive that results in deformation on the softer surfaces, thus leading to material loss. This detached material can be the broken grits from the softer surfaces, or they can be the protuberances on either or both of the surfaces (refer to Figure 2.3) [17]. Sometimes, the abrasive particles can be external or foreign elements that enter the tribosystem.

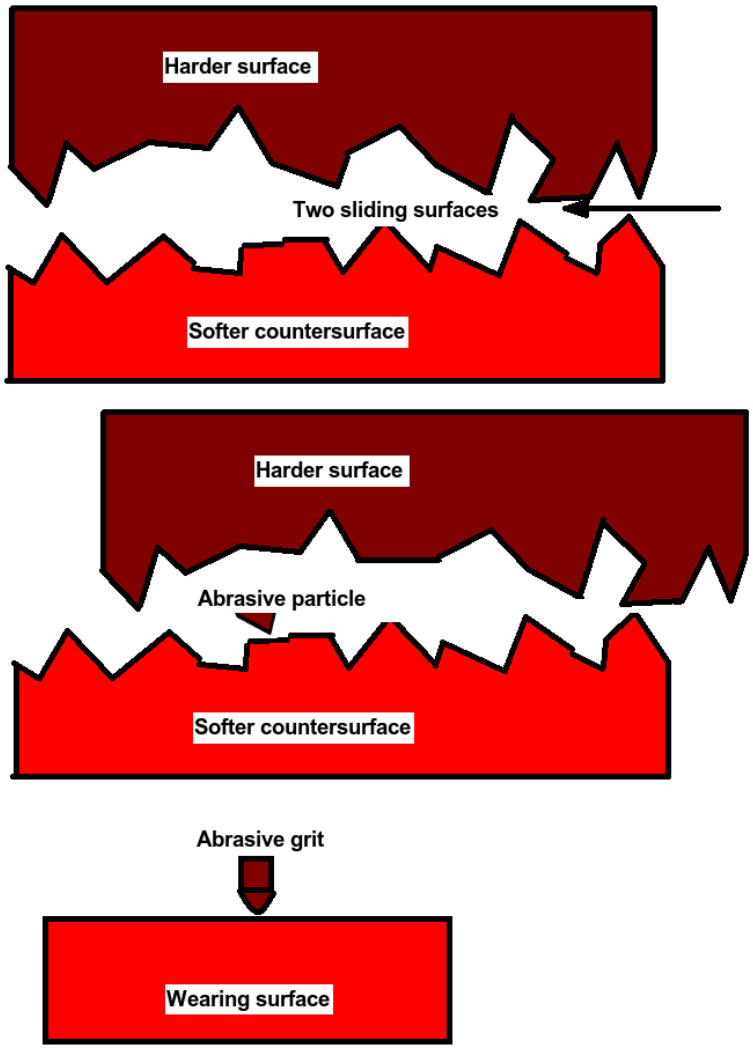

Figure 2.3: Abrasive wear that involves a two-body abrasion.

During abrasion, different physical processes are observed. The wear rate depends on the material properties and the operating variables [58]. The wear intensity is termed low or high, depending on the hardness values of the abrasive or the wearing surface.

Abrasive wear can be a two-body abrasion or a three-body abrasion, and the abrasion type depends on the number of surfaces in contact [6, 53]. In a two-body abrasion, an abrasive or harder material is free to move on the wearing or softer surface. In a three-body abrasion, material loss is observed when the abrasive particles

are moving between the solid surface and the wearing surface. The wear loss in a three-body abrasion is ten times less than what is seen in a two-body abrasion [14]. The reason is because of the smaller number of particles interacting with the wearing surface.

A two-body abrasion is very similar to a scratch test that involves grooving wear [9, 12]. This type of wear results in groove formation when a harder abrasive particle slides on the wearing surface, and the displaced groove material is pushed to the groove edges formed along the path traveled by the particle. The amount of wear loss is considered as the difference in the volume of the material displaced from the groove and the volume of material pushed to the groove edges. The scratched surface geometry is helpful in estimating the amount of material lost in a two-body abrasion. It is this type of wear that is commonly observed on the surfaces of a worn tillage tool. A number of analytical studies have been conducted with the objective of deducing an expression to determine the amount of material lost in abrasive wear with two-body abrasion [7]. Of the several approaches that have been proposed for calculating the wear rates, the concept of the material removal factor (f_{ab}) appears to be the most reasonable to use due to the ease with which the wear rates can be calculated from numerical simulations.

The material removal factor estimates the wear loss as the ratio of the difference in the volume of groove material and pile-up material to the volume of groove material. This is associated with the dominant mode of failure in a two-body abrasion. Previous wear-related studies classified the failure mode as [10, 47]:

- microploughing
- microcutting
- microcracking

In these failure modes, wear loss depends on the amount of material separated

from the groove material. In the microploughing mode of failure, surface deformation involves groove formation along the path traveled by an abrasive particle and the displaced material piling on the groove edges [11, 47]. During ideal conditions, there is no material separation from the wearing surface. Material loss is observed when many abrasive particles are acting simultaneously or successively. When the abrasive particles are passing successively, the material is plowed further onto the groove edges, or the pile-up material may separate due to fatigue failure [10]. Previous wear-related studies on metals have indicated that a small amount of the material displaced from the groove is removed as wear debris [5, 6, 8, 17].

For ideal microcutting, the volume of material lost in abrasion is the volume of material removed from the groove. The microcracking phenomenon is observed when highly concentrated stresses are imposed by the abrasive particles on a brittle wearing material. For ductile materials such as steel, the material loss is primarily due to the microploughing and microcutting modes of failure, and the transition from surface deformation to material separation depends on the material properties of the wearing surface and the operating conditions during the interaction [10].

To confirm abrasive wear, it is necessary that the deformed wearing surface shows groove formation and the displaced groove material accumulating on the groove edges. This behavior of a wearing surface is useful in investigating wear loss with the material removal factor (f_{ab}) and is helpful in estimating the wear loss. The material removal factor value is crucial in deciding the mode of failure because it takes into account the microploughing and the microcutting methods of failure [12, 47].

The advantage of using the f_{ab} factor is its sensitivity in evaluating the transition of surface deformation to material removal during a scratch test. When $f_{ab} = 0$, the microploughing mode of deformation is dominate; the volume of material displaced from the groove is equal to the volume of material pushed to the groove edges. The cutting mode is observed when $f_{ab} = 1$; the material removed from the groove is the

amount of wear loss.

With an increasing hardness of the wearing surface, the failure mode changes to microcracking. This failure mode is not found on the worn tillage tools since the tools need replacement much earlier than the occurrence of this failure mode. The primary reason for this is that the excessively worn tillage tools affect the power requirements and the wear of plowing assembly. In the next section, a comparison of the methods for estimating the wear loss is included from the various studies to quantify the material loss observed during abrasive wear in metals.

2.2 Wear Loss

Wear in metals is generally caused by a combination of adhesion, abrasion, surface fatigue, and tribochemical reactions. Abrasion is one of the dominant modes that results in material loss in metals [16]. In two-body abrasive wear, also called grooving wear, wear loss is dependent on the amount of material separated from the groove. For this, researchers have proposed a number of wear theories with the objective of quantifying the abrasive wear losses.

Rabinowicz provided an analytical expression, Equation 2.1, to estimate wear loss in a two-body abrasion [1]. This expression counts wear loss by the volume of groove material displaced by an abrasive particle [12]. This assumption is valid only for brittle materials where microcutting and/or microcracking is the only mode of surface failure, and material loss is equivalent to the volume of material displaced from the groove.

$$\frac{W_v}{s} = \frac{2\tan\alpha}{\pi}\frac{F_N}{H} \tag{2.1}$$

where, W_v is the volume loss due to wear, s is the sliding distance, F_N is the normal load on an abrasive particle, H is the hardness of the wearing surface, and α is the

attack angle of the wear particle (an abrasive particle is able to deform the wearing surface if its attack angle is greater than the critical angle).

Since the critical angle is associated with the geometry of an abrasive, equation 2.1 reduces to Archard's wear law given by equation 2.2:

$$\frac{W_v}{s} = \frac{k_{ab} F_N}{H}. \tag{2.2}$$

Here, k_{ab} is the wear coefficient, which is equivalent to $\frac{2\tan\alpha}{\pi}$ in equation 2.1.

In equation 2.2, only one material property, the hardness, is considered; however a two-body abrasion involves wear and friction in the absence of lubrication. In addition, the amount of material loss depends on the material properties, the microstructural parameters, and the operating variables [5]. Also, Archard's wear law is based on the critical attack angle (α_c), and the expression fails to predict wear loss either when the microploughing mode of deformation is dominant or when there is a sharp transition from material deformation to material separation after a certain value of the critical attack angle.

The abrasive wear coefficient, k_{ab}, is dependent on the shape, size, type and distribution of the abrasive particles [16], on the wearing material properties and the mode of interaction between the abrasive particles and the wearing material. For a spherically shaped particle, wear intensity is dependent on the depth of penetration and the tip radius of an abrasive particle.

Zum Gahr's work discusses a set of analytical expressions that can be used in estimating the wear loss in a two-body abrasive wear. These equations [10, 47], instrumental in calculating the losses analytically as well as numerically, are:

$$W_{l/s} = \frac{W_m}{\rho A s} \tag{2.3}$$

and

$$W_{v/s} = \frac{W_m}{\rho s} = \frac{W_v}{s} \tag{2.4}$$

where, W_l is the linear amount of wear (m), $W_{l/s}$ is the linear wear intensity, W_m is the mass loss due to wear, $W_{v/s}$ is the volumetric wear intensity, ρ is the density of wearing material, A is the wearing area, and s is the length of the wear path. These expressions are valuable in estimating wear losses because the calculations include the material behavior.

Figure 2.4 depicts the basis for the classical ploughing theory, one of the wear theories that is helpful in estimating the f_{ab} factor. The factor is calculated from the groove material volume and the displaced groove material volume piling on the groove edges. In this theory, the f_{ab} factor is instrumental in associating the material properties with the wear loss.

The classical ploughing theory (refer to Figure 2.4) [14, 19], based on a scratch test, provides an expression for the f_{ab} factor. This factor value is an indicator of the dominant mode of failure in a two-body abrasion.

$$f_{ab} = \frac{A_g - (A_{p1} + A_{p2})}{A_g} \tag{2.5}$$

where, f_{ab} is the material removal factor

A_g is the volume of material displaced from the groove

$(A_{p1} + A_{p2})$ is the total material piling on the groove edges

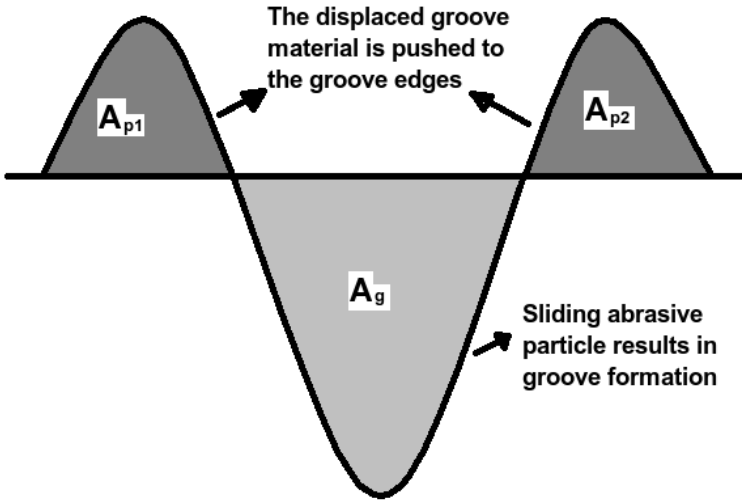

Figure 2.4: The classical ploughing theory.

Previously, studies have included the effects of the shape of an abrasive on the wear loss, and it has been found that wear loss increases with the increasing penetration depth of an abrasive. This observation is in agreement with the experimental studies. The amount of wear loss in a scratch test, when combined modes of failure (i.e., microploughing to microcutting) are dominant, is expressed in the following equation [6, 10, 17].

$$W_{v/s} = \frac{W_v}{s} = f_{ab} A_g \tag{2.6}$$

where, $W_{v/s}$ is the volumetric wear intensity, W_v is the volumetric wear loss, s is the distance traveled by an abrasive in a scratch test, f_{ab} is the material removal factor, and A_g is the groove area.

In the field of tribology, a number of studies (experimental and numerical) have been conducted to estimate the wear loss in metals using laboratory tests. In addition, a good amount of work has been done to calculate wear loss using a numerical

technique. It is interesting to note that many researchers have validated the numerical predictions with experimental observations.

Fang et al. investigated wear loss in metals using the finite element method and found their predictions following a similar trend observed in the laboratory tests [49]. Their work shows that the material removal factor (f_{ab}) is an important estimator of the wear and the wear rates of the metallic surfaces experiencing a two-body abrasion. To determine the f_{ab} factor, it is necessary to measure the surface deformation of a wearing surface.

The importance of the f_{ab} factor was earlier established by Zum Gahr who did analytical studies and found that introducing the factor into wear equation results in a better approximation of abrasive wear losses [10]. Later, Fang et al. have confirmed that it is very difficult to measure the deformed surface geometry, but the finite element method provides an efficient method to measure the geometry by modeling the two-body abrasion as a scratch test [50]. Their work indicate that numerical results using the concept of the f_{ab} factor turned out to be in close agreement with the laboratory observations.

Wear related studies indicate that a number of variables are involved during the abrasive wear of metals. The variables such as material removal factor; abrasive particle size, shape, and indentation depth, hardness, material properties, and speed are quite influential during two-body abrasion. For this reason, a review of previous studies has been conducted to identify the important factors that are useful for a complete study on abrasive wear. It has been found that the following factors are instrumental in investigating wear loss in a two-body abrasion.

2.2.1 Material Removal Factor

The material removal factor is helpful in determining the amount of material loss from a wearing surface. The importance of the factor value is to establish the primary mode of failure observed on a wearing surface. Previous studies indicate that

the wear loss in a two-body abrasion is dependent on the mode of failure mechanism occurring on the wearing surface, when an abrasive interacts with the surface.

For $f_{ab} = 0$, the microploughing mode of surface failure is predominant and indicates permanent deformation on the surface; however material loss is dominant when the factor value is greater than zero [26, 49]. This transition from one failure mode to the other indicates material loss during two-body abrasion.

Therefore, the volume difference in the material displaced from the groove and the material piling on the groove edges is approximated as the amount of wear loss in a two-body abrasion. For lower f_{ab} values, microploughing is dominant and indicates more material deformation than wear loss [12, 13, 26].

2.2.2 Abrasive Particle Size

For wear related studies involving two-body abrasion, the amount of wear loss is found to be dependent on the size of an abrasive particle [14, 26, 49]. It has been observed that wear loss in metallic materials increases with increase in the particle sizes. In the literature, references are found that show the wear loss is affected for a range of abrasive particle sizes. Fang et. al found that numerical results indicate negligible change in the f_{ab} factor values when the abrasive particle diameter is greater than 500 microns [5, 13, 14, 26, 43, 49].

However, the particle size is also associated with the number of particles interacting with the wearing surface [2, 57]. Generally, lower wear rates are observed with an increase in the particle size which results in reduced number of abrasives interacting with the tool surface. Consequently, the magnitude of forces is distributed on the number of particles interacting with the softer material surface. Since increase in particle size results in a lower number of abrasives interacting with the surface, it is seen that the force magnitude on an individual particle is higher than what is observed with smaller particle sizes. Therefore, wear loss is associated with the particle size.

In a typical soil, the particle size can be as small as 0.002 mm or greater than 2.0 mm. Since the abrasive wear loss is affected by the particle size, the two-body abrasion tests provide a useful method to conduct the wear related studies during soil-tool interaction.

2.2.3 Abrasive Particle Shape

Gahlin et al. confirmed that sharp particles do not show critical particle size effects. In fact, blunt particles predict a great variation in wear rates for different particle sizes [30]. Also, Hamblin et al. found that the wear rate is affected by the particle shape, but it is very difficult to measure the physical geometry of quartz particles [24]. Since determining a physical form of an abrasive particle is tedious, the shape factor is usually ignored. Additionally, Terzaghi et al. claims that the size of a soil particle is estimated by comparing it with the time taken by a spherical particle to sink in a water medium. For this reason, numerical studies on abrasive wear involving two-body abrasion are generally carried out with the assumption of spherically shaped abrasive particles [53].

2.2.4 Indentation Depth

In a two-body abrasion, involving grooving wear, the groove depth is important in describing the wear resistance of a wearing material surface [12]. The indentation depth by an abrasive particle is affected by the number of particles coming in contact with the softer surface [50].

Since an increase in particle size leads to a higher load on an individual particle, it has been observed that a higher groove depth is visible on the deformed surface [15]. Therefore, for the same magnitude of the forces existing in the system, high wear rates are observed when the f_{ab} factor is calculated with incremental indentation depths [22]. The calculated f_{ab} factor values can be used to monitor the effects of indentation depth on wearing properties [49]. Jacobson et. al. found that the wear

loss is linearly dependent on the indentation depth [14].

2.2.5 Scratch Distance

Scratch distance is one of the factors that is useful in exploring abrasive wear. The factor is important because the deformed surface is an indicator of wear behavior usually recognized in terms of a groove and ridges formed along the distance traveled by an abrasive sliding on a wearing surface. Previous studies investigating abrasive wear using a scratch test indicate that the groove depth and ridge height become stable along the scratch distance after an initial increase in the deformed geometry of a wearing surface [22, 38, 49, 50].

This observation can be linked with the tool wear during tilling operations as maximum wear loss is observed primarily for a distance of 25 mm to 40 mm along the tool length. Since a two-body abrasion test involves the distance traveled by a single abrasive, the distance traveled by a soil particle can be related to the scratch distance.

2.2.6 Hardness

Wear rate is linearly proportional to hardness [8]. Also, wear involves heat, which is usually due to friction between an abrasive and a wearing surface, and is dependent on the material properties. Frictional heat can be ignored for a two-body abrasive wear study involving a single abrasive particle interacting with the wearing surface but comparing the effect of material hardness provides a qualitative support to investigate the effects of friction on wear rates.

The particle hardness does not affect the wear rates, as long as the abrasive particles are harder than the counter-surface. The difference is observed only when the wearing material hardness is significantly lower [50, 57]. The hardness property is important for wear studies, especially materials with high work-hardening, because hardening affects the surface deformation [53].

The maximum deformation is observed on the surface surrounding an abrasive particle sliding on the wearing surface. Therefore, it is important to include the work hardening for the numerical investigation of wear losses. Otherwise, erroneous results are expected due to a decrease in the height of pile-up followed by an increase in the pile-up thickness [38]. Accordingly, the intensity of surface deformation and groove formation is dependent on the hardness of the wearing material.

Garrison found that a decrease in the pile-up height and an increase in the groove width is a function of the linear hardening property of a wearing material. For the materials having low work-hardening, microploughing is the dominant failure mode [11].

2.2.7 Groove Geometry

The amount of material loss is dependent on groove size. A smaller groove size indicates that the major portion of the groove material is displaced/removed by the smaller abrasive particle sizes moving on the softer surface [14]. Since surface failure is observed in terms of groove and pile-ups, the failure mode is dependent on the ratio of height to width of the pile-up formed along the scratch distance covered by an abrasive particle. The study of groove and pile-up geometry is quite useful to understanding the effects of the multiple pass on the deformed surface. The effects of abrasive particles following other particles that have already scratched the wearing surface is important [11].

A worn tool surface indicates groove formation along the tool length. On the tool surfaces, the pile-up formation is not observed on the groove edges, because the displaced groove material is removed by either fatigue that results in material loss from the ridges or by other soil particles moving along the tool surface. Also, it is required to understand the effects of the factors that are associated with the two-body abrasion to conduct the numerical studies and estimate the tool wear losses.

2.3 Soil-Tool Interaction

The complexities associated with the soil-tool interaction make the wear related studies difficult specifically using a numerical technique [4, 34, 45]. A survey of literature indicates that although numerical techniques were implemented to model the soil deformation caused by the tool movement, very little attention was given to understand/estimate tool wear during the plowing operation [46, 55]. Some of the numerical studies compared pressure developed on a tool surface used for soil plowing [28, 56, 64, 68]. It has been observed from these studies that tool wear was associated with the critical points on the tool surface subjected to excessive stress during soil plowing [35]. However, these studies were conducted primarily to identify the soil behavior due to the movement of a tillage tool and compared the forces generated on the tool surfaces due to soil deformation [44, 51, 64]. The failure zone was predefined along the path travelled by the tool against the soil block, and the soil deformation was modeled using various constitutive material models [5, 54, 65]. In addition, parametric studies were done using the data acquired from field tests in terms of tool forces, and the variation in tool forces was considered to understand the effect of operating variables on tool wear [23, 29, 34, 35, 60].

Natsis et al. designed experiments to predict variations in tool wear rates for a different set of soil material properties, such as hardness of soil particles, moisture content, and plowing conditions [66,69]. Of the different variables affecting the tillage process, the primary parameters affecting the tool wear are discussed below.

2.3.1 Soil Properties

Abrasive wear of a tillage tool is influenced by soil properties, such as moisture content, density, and hardness [18, 41, 61, 66]. Natsis et al. showed that the rate of tool wear depends on the soil moisture content which is further dependent on the geographical location and the soil type [18,61,66]. However, in sandy soils, the quartz particles are exceptionally hard [69] and scratch the tool surface, thus enhancing the

Figure 2.5: Two different views of a worn tillage tool surface from field tests.

tool material loss with some contributions due to tribochemical wear [67]. Also, the abrasion of a tillage tool surface reduces when the soil is dry and firm [68].

2.3.2 Soil Particle Size and Indentation Depth

Soil is a non-homogeneous mixture of organic and inorganic materials. The physical constituents of soil make it a challenge to predict soil behavior that is subjected to external loading in different fields, such as construction, agriculture, and other earth moving activities. A branch of science, soil mechanics provides a platform to link the painstaking experimental findings with the classical theories of elasticity and plasticity [20].

Terzaghi et al. [20] classified soil based on its index properties. The index properties of a soil are classified as follows:

1. Soil grain properties

    (a) Size and shape of the grains in sandy soils

        i. Very coarse and coarse fractions of soil:soil particle size greater than 0.06 mm

ii. Fine fraction: soil particle sizes ranging from 0.002 mm to 0.06 mm

iii. Very fine fraction: soil particle sizes less than 0.002 mm

(b) Mineralogical character of the smallest grains in clay soils

2. Soil aggregate properties

(a) Cohesionless soils: relative density

(b) Cohesive soils: consistency

For tool wear studies, it is important to include the effects of size, shape, and hardness of soil constituents [3]. Since the particle shapes and sizes are difficult to measure due to the impracticality of it, often, the particle shapes are treated as spherical with an "equivalent" radius based on the size of the particle. Previous studies by Natsis et al. indicate that sand particle sizes greater than 0.01 mm influence the rate of tool wear [66]. The particle size distribution of the soil considered in the experimental studies of the Surfaces and Tribology group in Colombia is shown in Figure 2.6. These studies indicate that the large size soil particles, sand and gravel, are primarily responsible for wear in tillage tools.

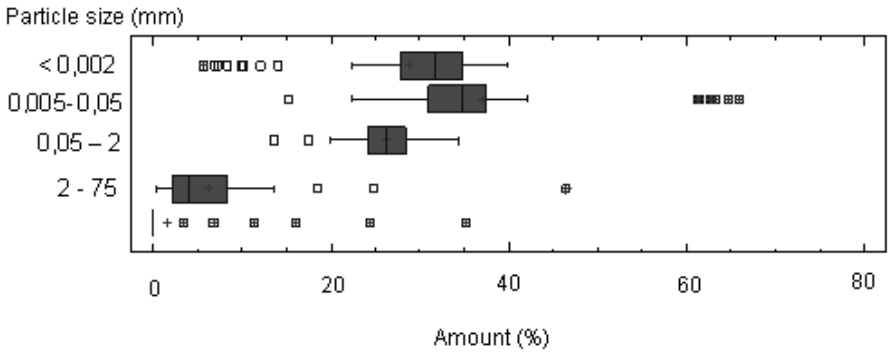

Figure 2.6: Particle size distribution of the soils taken for the experimental study on tool wear.

Figure 2.7 shows the profile of a surface of a used tillage tool. This profile is again from the Surfaces and Tribology group in Colombia. As can be seen in this

figure, the surface undergoes significant wear due to tilling and some of the scratches are significantly deeper. The differences in scratch geometries are due to the shape of the particle, size of the particle and also the momentum with which a particle impacts and slides along the surface. As mentioned above, the shape of a particle is usually taken to be spherical for modeling purposes. In addition, the scratch depth is also prescribed as the initial indentation depth for the two-body abrasion modeling purposes.

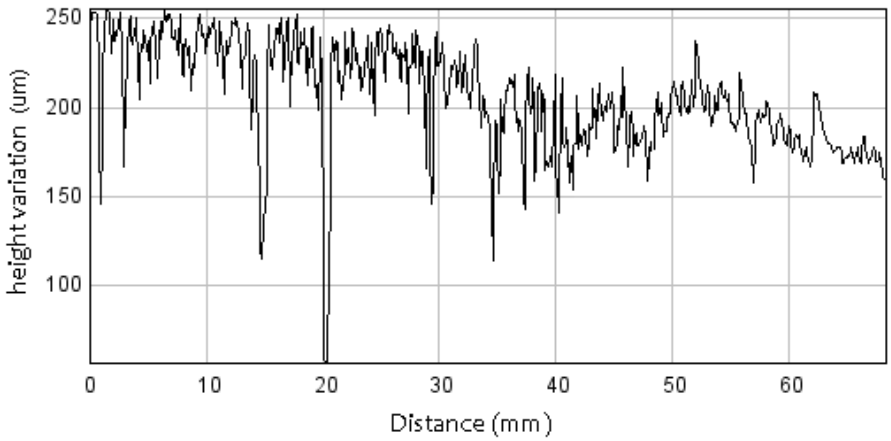

Figure 2.7: A profilometric graph of a tool surface showing an average of 5-6 scratches per centimeter.

These observations provide sufficient information about some of the controlling parameters that are part of a tillage system, and useful for making some reasonable assumptions required to model the soil-tool interaction to further the understanding of tool wear.

2.3.3 Tilling Parameters

U Er. et al. found tillage speed to be one of the crucial factors affecting tool wear rates during tillage process [40, 41, 56, 61]. In addition, their work and field tests indicate that tool wear is also affected by the plowing depth [68].

Tool wear is dominant in those sections of tool surface where the magnitude of

stress is relatively higher. This is primarily due to friction forces generated between the tool surface and soil material during tilling. Abo-Elnor et. al suggested that excessive stresses are found in some parts of a tillage tool that are subjected to inertial forces due to soil dynamics [45]. Interestingly, some field studies indicate that tillage speed has negligible effect on the magnitude of the tool forces [18]. Also, it has been discovered that tool wear is affected by the tool cutting angle, the angle formed by a tillage tool with respect to the horizontal axis of soil strata [33, 48].

2.3.4 Tool Material Hardness

Wear resistance of tillage tool material is dependent on its hardness value [18, 61, 66] but raising the material hardness beyond a particular limit makes the material brittle. To avoid the microcracking mode of failure in tillage tools, the material hardness property has to be in a range to prevent the sudden tool failure. For this reason, tensile tests were conducted to determine the mechanical properties of the tool material which are useful to determine the tool surface deformation.

2.3.5 Mechanical Properties of Tillage Tool Material

Commercial tillage tools are made of DIN 30MnB5 alloy steel. The mechanical behavior of this steel was obtained using tensile tests. These tests were conducted at room temperature by the Surfaces and Tribology group at the National University of Colombia-Medellin.

The nominal stress vs nominal strain curves are shown in Figure 2.8) for the steel heat-treated at three different temperatures. The corresponding true stress vs true strain curves are shown Figure 2.9. The tool material that is considered in the present work is that shown in green.

The observations from previous work and the field studies are incorporated in this dissertation to develop finite element models of tool wear (as a two-body abrasion problem) and soil-tool interaction. These models are used to study tool wear and

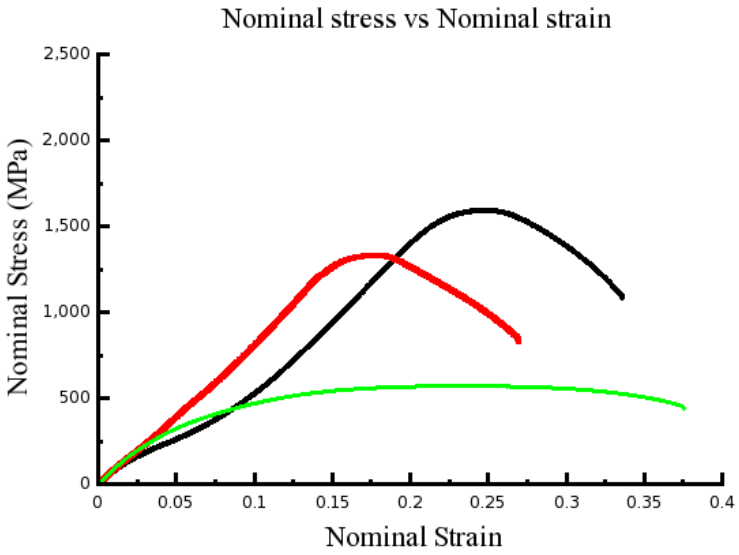

Figure 2.8: Nominal stress vs nominal strain curves for the tillage tool material heat-treated at three different temperatures.

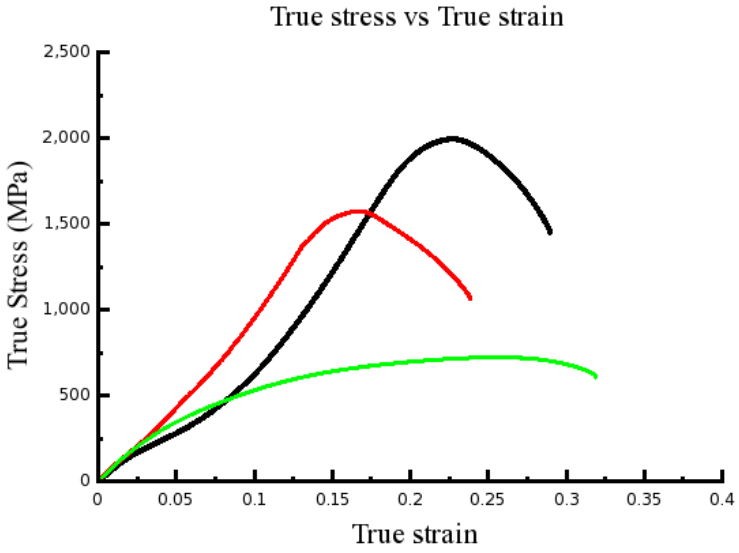

Figure 2.9: True stress vs true strain curves for the tillage tool material heat-treated at three different temperatures.

estimate power consumption and its dependence various tilling process parameters.

The specific objectives of this study are to:

- develop finite element models to predict tool wear during tilling operations.
- develop finite element models to simulate tilling process and predict power re-

quirements.

- validate the models with experimental results.
- use these models to study the effect of various parameters on tool wear and power needs.

The finite element studies and their implementation to predict wear related tool losses during soil tillage require that an appropriate numerical scheme be selected to model the complex behavior of the soil and the tool surfaces during soil-tool interaction. In the following chapter, a brief discussion is made on the numerical scheme that has been selected to simulate the two-body abrasion and soil-tool interaction.

CHAPTER 3: THE EXPLICIT METHOD IN ABAQUS

As mentioned in the previous chapter, the finite element method is used to study tool wear and soil-tool interactions. The soil deformations are large during tilling. The tool wear due to soil particles also involves large inelastic deformations prior to the material loss. Since the equations that govern these deformations are highly nonlinear, the commercial finite element package, ABAQUS, is used to study both tool wear and soil-tool interactions. Both the implicit and explicit methods can be used for solving these problems where dynamic effects play a significant role. In the present study, the explicit method is chosen over the implicit method since the nonlinear nature of the problems and the small time-increments needed make the implicit methods impractical.

As discussed in the previous chapter, a few finite element studies have been conducted previously to study soil-tool interaction. Many of these studies were based on custom-built, in-house codes that had limited capabilities [64] and numerical issues. In some studies, to prevent errors due to severe element distortion, the tool displacement was restricted to small distances [41]. A robust and well-tested software such as ABAQUS provides superior capabilities that many of these in-house codes lack. Some of these are the ability to handle large deformations, a large number of constitutive laws for material behavior, various friction models and the ability to use one's own models for material behavior and friction. Furthermore, adaptive meshing to handle large element distortions is also available. In the following, the numerical integration scheme that ABAQUS/Explicit uses and its adaptive meshing capabilities are discussed.

3.1 ABAQUS/Explicit Algorithm

The standard displacement-based finite element method for the equations governing the dynamic behavior of solid materials leads to the system of equations

$$\mathbf{M}\ddot{\mathbf{d}} + \mathbf{I}(t) - \mathbf{P}(t) = \mathbf{0}. \tag{3.1}$$

Here, $\mathbf{M}$ is the mass matrix, $\mathbf{d}$ is the nodal variable vector and $\mathbf{I}$ is the internal force vector and $\mathbf{P}$ is the external force vector. The dots indicate differentiation with respect to time. In ABAQUS/Explicit, the global mass matrix is first reduced to a lumped mass matrix which is diagonal. The diagonal lumped mass matrix makes inversion of the mass matrix unnecessary. The time derivative terms are discretized using an explicit centered finite difference scheme as follows:

$$\dot{\mathbf{d}}^{i+\frac{1}{2}} = \dot{\mathbf{d}}^{i-\frac{1}{2}} + \frac{\Delta t^{i+1} + \Delta t^{i}}{2}\ddot{\mathbf{d}}^{i} \tag{3.2}$$

and

$$\mathbf{d}^{i+1} = \mathbf{d} + \Delta t^{i+1}\dot{\mathbf{d}}^{i+\frac{1}{2}}. \tag{3.3}$$

Here, the superscript i denotes the increment number and $i \pm \frac{1}{2}$ denote midincrement values.

The acceleration term $\ddot{\mathbf{d}}^{i}$ is determined from 3.1:

$$\ddot{\mathbf{d}}^{i} = \mathbf{M}^{-1}\left(\mathbf{I}^{i} - \mathbf{P}^{i}\right).$$

Since the mass-matrix is diagonal, it is not necessary to explicitly invert it. Thus, it is not necessary to solve a system of equations and no iterations are needed. Furthermore, the internal force vector can be formed without forming the global stiffness

matrix.

Since this method is not self-starting, the initial conditions on displacement and velocity along with the discrete balance of linear momentum equations are used to generate the value of $\dot{\mathbf{d}}^{-\frac{1}{2}}$. More details on this can be found in ABAQUS user manuals.

In the explicit scheme, although much simpler to use than the implicit schemes, the time increments cannot be taken to be arbitrarily large. The time-increment must satisfy a stability criterion given by

$$\Delta t \leq \frac{2}{\omega_{\max}} \left(\sqrt{1+\xi^2} - \xi \right) \tag{3.4}$$

where ξ is a fraction of critical damping in the highest frequency mode of the entire model. However, a conservative estimate of the time-step can be obtained by considering the highest frequency mode of an element. For example, in the absence of damping, the maximum time increment allowed is written as

$$\Delta t \leq \frac{2}{\omega_{\max}^{\mathrm{e}}} \tag{3.5}$$

where the superscript e represents element e. The timestep Δt is calculated for all the elements and the minimum amongst them is taken as the allowable time increment. The maximum frequency for each element e can be estimated from a characteristic element dimension and an effective dilatational speed of the material. The characteristic element dimension depends on the element area and the element gradient operators [71].

Thus, although explicit schemes are easier to implement, the limitation on the stable time-step often means that a large number of time increments are needed to reach a solution state at a desired time. However, when there are a large number of degrees of freedom in a given problem, explicit schemes are often advantageous over

implicit schemes.

ABAQUS/Explicit automatically chooses the stable time increment and there is no need in general on the part of the user to specify the time increment. In addition to stable time increments, ABAQUS also uses bulk viscosity in Explicit to minimize the ringing phenomenon that is usually associated with the high frequency components. The bulk viscosity damps the high frequency components out. Consequently, caution needs to be exercised in using the bulk viscosity. However, the default values are such that the solution is not polluted by the artificial damping of the high frequencies.

3.2 Adaptive Meshing

In both the problems that are considered in the present work, the deformation on the tool surfaces or in the soil, is very large. To reduce the errors due to the severe element distortions caused by the large deformations, ABAQUS provides a technique-adaptive meshing-that maintains the quality of the mesh throughout the analysis.

This meshing technique is particularly helpful in reducing distortion errors in nonlinear dynamic analysis problems, which involve large deformation and material removal during analysis. This technique can be used for two-dimensional (plane strain, plane stress, and axisymmetric) and three-dimensional problems. In addition, adaptive meshing is applicable for nonlinear geometry, where mesh movement is independent of material deformation. To implement this technique smoothly, it is important that the model is assigned first-order solid elements with reduced integration.

Generally, adaptive meshing is associated with the new mesh formation and the remapping of solution variables from the older mesh to the new mesh. Adaptive meshing is performed in the assigned mesh domain defined by a boundary region. This region can be Lagrangian, sliding, or Eulerian. Often, the region is assigned automatically in ABAQUS, but other regions can be created by assigning boundary

conditions, loads, and surfaces.

In 2D, the regions are separated by corners called boundary region edges. These edges can be Lagrangian or sliding. In the Lagrangian mode, nodes move along the edge, but the material is not able to move past the edge. In the sliding mode, the edges can slide freely over the material. In ABAQUS/Explicit, Lagrangian boundary regions are usually created by the software itself, except on the contacting surfaces. In this mode, the mesh will follow the material in the direction normal to the surface of the boundary region and boundary region edges. The boundary region from inside is comparable to the mesh patch that is following the material. Nodes are free to move both on or inside the patch.

The Lagrangian corner moves with the material and is nonadaptive [71]. In the case of the sliding mode, boundary regions have a sliding edge. This meshing patch moves freely and is independent of the underlying material; however the Eulerian boundary regions allow the material to flow across its boundary. The region assignment is defined on the exterior of the model. In ABAQUS, the Eulerian boundary region is specified externally. Otherwise, the default method is the Lagrangian boundary. For material movement across the mesh, the mesh movement is constrained from moving in a direction normal to the material surface.

To overcome default parameters, ABAQUS provides the user with certain freedoms to change the mesh controls, depending on the analysis type used to reduce element distortion errors. These controls include defining frequency or intensity. Of these two controls, it is important to change the intensity, which is modified by selecting an appropriate number for the mesh sweeps and the advection sweeps. In the mesh sweep, the element distortion error is reduced by relocating the nodes, which further depends on the position of neighboring nodes. In ABAQUS, the explicit scheme does not allow the user to define the number of advection sweeps for each adaptive mesh increment. This calculation is done independently by the software because this

technique involves remapping the new mesh with the solution variables from an older mesh; this occurs once all the mesh sweeps for an increment are completed. However, the technique is quite useful in reducing the numerical issues and in maintaining the mesh quality throughout the analysis.

3.3 Contact

In the present work, two specific problems are considered. The first is a wear-study of tillage tools and the second is the calculation of power consumption during tilling. Both of these involve soil particle(s) moving against the tool's surface. Consequently, it is important to consider friction between the soil and tool. In ABAQUS, contact is specified through the interaction module. A number of friction models (including user supplied) are available to define contact between surfaces. In the present work, the interaction between the two materials is modeled with the basic Coulomb friction model, relating the shear stress across an interface to the contact pressure between the contacting surfaces. According to this model, the contacting surfaces will stick to each other for a certain value of shear stress, but beyond the critical value the sliding will start. Coulomb's law states that this critical value of shear stress (τ_{cr}) is a fraction of contact pressure (p), and the related expression is given as

$$\tau_{cr} = \mu p \tag{3.6}$$

where, μ is the friction coefficient that defines the transition between sticking and sliding. This model assumes that the friction is isotropic (i.e., same in all directions).

CHAPTER 4: TILLAGE TOOL WEAR

In this chapter, finite element models to study tillage tool wear are presented. The classical ploughing theory and the concept of material removal factor are used to predict tool wear. The finite element models are presented and the numerical results are validated against the experimental observations of tool wear. Following the validation, various parametric studies involving tillage parameters are conducted and the results from these studies are also presented.

4.1 Two-body Abrasion

Tool wear during tilling operations can be due to several mechanisms: abrasion, chemical action, fretting and erosion. The focus of the present work is on tool wear due to abrasion since experimental studies indicate that this is the most dominant mechanism. Abrasive wear results when a hard particle slides against a softer material and causes material loss. The harder particles can have both translational and rotational motions that contribute to wear. However, in soil-tool interaction, due to the translating motion of the bulk material, the translational component is dominant. Furthermore, as a first approximation, tool wear can be thought of as that due to cumulative effect of many particles scratching the tool surface where the action of each particle is independent of the actions of the other particles. This assumption allows one to investigate tool wear using the two-body abrasion models where a single particle slides against a surface at a prescribed speed and prescribed initial indentation depth [38]. This critical assumption also allows one to study the effect of various parameters in tillage operation on wear within the context of the two-body abrasion models.

The two-body abrasion process is modeled using the commercial finite element software package ABAQUS/Explicit. The model assumptions and steps taken to carry out the numerical simulations in ABAQUS are discussed next.

4.1.1 Geometry

A single soil particle is considered as a cylindrical body with a hemispherical tip. In geomechanics, a soil particle size, especially sand particle, is measured by performing wet tests. In this test, a sand particle is allowed to move in a water medium and the time taken by it to reach the bottom surface is measured. A sand particle size is estimated from the equivalent time taken by a spherical shaped particle to sink in a water medium [20].

For modeling purposes, the soil particle is considered to be a rigid body. This assumption is based on the fact that soil particles are made of quartz, which is one of the hardest materials capable of scratching steel and its alloys. Additionally, this assumption has been validated by comparing simulation results when the soil particle is considered as a deformable body. Furthermore, the soil particle considered is sand with sizes falling in the categories of large and very large which range from 0.5 mm - 1 mm and 1 mm - 2 mm respectively. In this work, the large and very large sand particle sizes have been considered to account for the tool material loss.

The tillage tool is modeled as a rectangular block with dimensions 3.0 mm $\times$ 1.2 mm $\times$ 1.2 mm (refer to Figure 4.1). For large sand particle sizes, the block size dimensions are similar to those used by Fang et al. [49]. The block size dimensions are large enough so that the boundary effects do not influence the stresses and displacements in the vicinity of the scratch.

For very large sand particle sizes (1.0 mm to 2 mm), the block size is taken to be 5.0 mm $\times$ 3.2 mm $\times$ 3.2 mm (refer to Figure 4.2). Again, the block size is chosen so that the scratching process is not influenced by the boundary effects. It is worth noting that these dimensions are much smaller than those of a typical tillage tool.

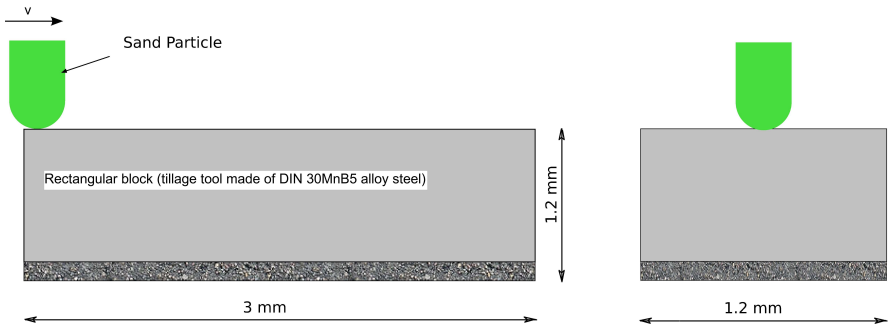

Figure 4.1: A 2D schematic that shows the front and side views of a sand particle scratching the tool surface with one of the large sand particle sizes (0.5 mm).

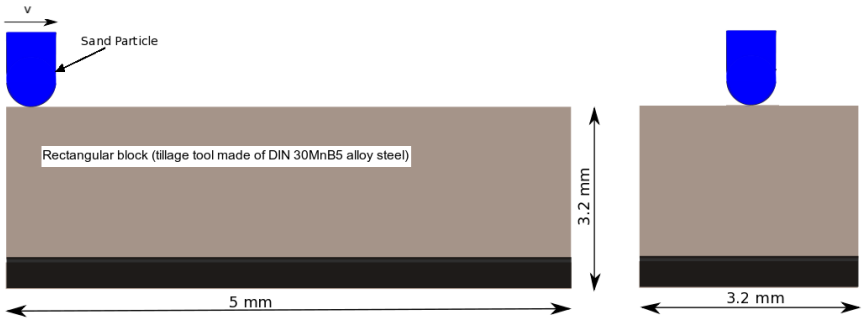

Figure 4.2: Figure shows a 2D schematic of a very large sand particle (1.1 mm) in contact with the tool block.

The sliding of the sand particle over the rectangular steel block is modeled as follows: first, the sand particle indents the steel block with a specified indentation depth and, then, the particle is moved along the surface of the block at a prescribed speed simulating scratching of the surface. The particle is assumed to indent the block symmetrically. This, coupled with the symmetry of the geometries involved in the problem, requires only half of the sand particle and tool block to be modeled in the numerical simulations (see Figures 4.1 & 4.2).

4.1.2 Constitutive Model

The rectangular block is made of DIN 30MnB5 steel alloy which is the tillage tool material. As mentioned earlier, the soil particles have a significantly higher hardness than the tool material. For this reason, the soil particles are treated as rigid particles.

The mechanical behavior of the tool material is assumed to be governed by the classical J2 flow theory with isotropic linear hardening and an associative flow rule. During tool wear, the temperature effects can be significant due to local heating resulting from friction and large deformations. However, due to the lack of availability of data for inelastic and thermal behavior of the material, these effects are not taken into account. The elastic behavior is defined by Young's modulus (E) and Poisson's ratio (ν), and plastic behavior with linear hardening involves yield stress (σ_y) and corresponding plastic strain (ε_p). The specific material properties are shown in Table 4.1.

Table 4.1: Elastic and plastic properties of a DIN 30MnB5 steel.

Elasto-plastic Properties	
E	210 GPa
ν	0.3
σ_y @ $\varepsilon_p = 0$	510 MPa
σ_y @ $\varepsilon_p = 0.35$	710 MPa

4.1.3 Load Steps and Contact

To model the scratching process, initial contact between the sliding particle and the block surface is established as shown in Figure 4.3. The contact between the sand particle and the block is assumed to be frictionless [39]. Simulations run with frictional contact indicate that friction does not have a significant effect on the numerical results, which is an observation consistent with the conclusions observed from the work of Fang et al. [50]. Since the scratching process involves large deformations of the block, contact between the sand particle and block surface is assigned with optimal contact control parameters to reduce numerical errors and computational times.

Once contact is established, the scratching process is modeled in three load steps. In the first step, the sand particle makes an indentation of a specified depth in the steel block. In the second step, the particle is given a horizontal speed so that a

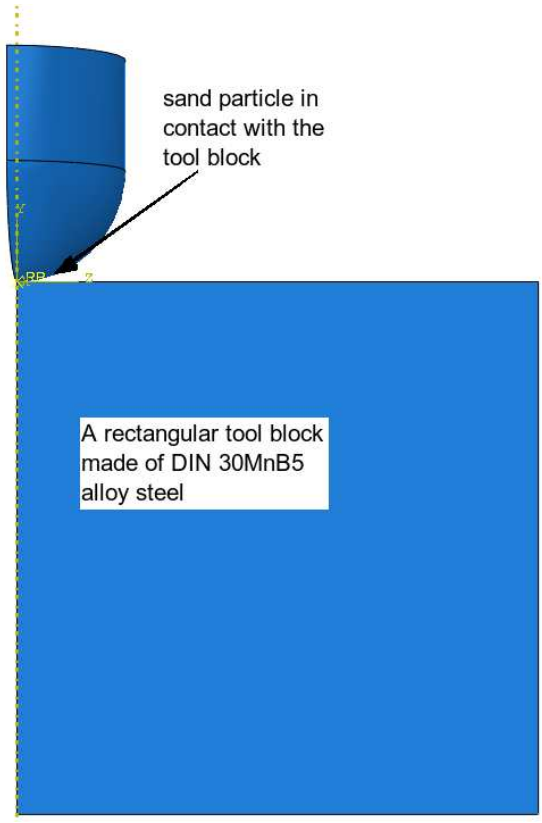

Figure 4.3: Initial load step to establish contact between the sand particle and the tool block.

scratch of a specified depth and length is made in the block [47]. In the third step, the indenter is withdrawn gradually so that elastic recovery takes place in the block. It is worth noting that the indentation depths are typically about one-tenth of the particle diameter. These depths lead to inelastic deformations and, therefore, groove formation (scratch) on the surface of the block.

4.1.4 Boundary and Initial Conditions

The block is fixed at the bottom and symmetry boundary conditions are applied on the symmetry plane identified by ABCD in Figure 4.4.

For the sand particle, which is treated as a rigid body, an initial vertical displacement equal to the indentation depth is given in the first step. In the second step, the particle is given a horizontal speed of 1.2 m/s while keeping the vertical displace-

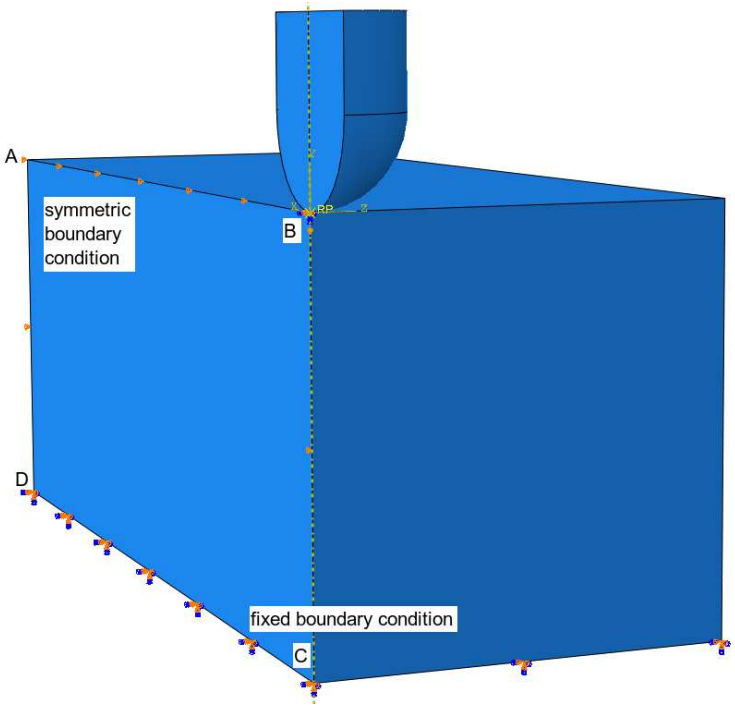

Figure 4.4: Boundary conditions used in the numerical simulations of the sand particle sliding on the tool surface.

ment at the indentation depth. This amounts to scratching the surface of the block. The block length is chosen so that sliding is achieved after an initial unsteady phase. This length is established by carrying out numerical simulations for different scratch lengths and choosing the smallest length that gave steady-state results. The final displacement constraint on the particle is given in the third step when the scratching is complete. In this step, the particle is withdrawn vertically from the block surface.

4.1.5 Meshing

The rigid sand particle is modeled with discrete R3D4 (rigid four-noded, three-dimensional quadrilateral elements) elements, and the rectangular block is discretized using C3D8R (deformable eight-noded, three-dimensional solid elements with reduced integration) elements. These three dimensional linear continuum solid elements are 8 noded linear brick elements with a reduced integration having 8 degrees of freedom. In this first order element type, 4 nodes are located on the corners of the element,

and the shape functions are linear in each of the local coordinates.

The tool block is discretized with approximately 90,000 elements for sand particle sizes in the range of 0.5 mm to 1 mm Biased meshing is used for the block so that a fine mesh is present in the scratch region and a coarse mesh is present away from the scratch region. To model tool surface deformation, when the wear analysis involves very large sand particles (1 mm to 2 mm), the block is discretized with 312,500 elements (refer to Figure 4.5). The element density is set higher to achieve a better approximation for the scratch region. Results from simulations with finer mesh sizes for both the cases show no appreciable differences.

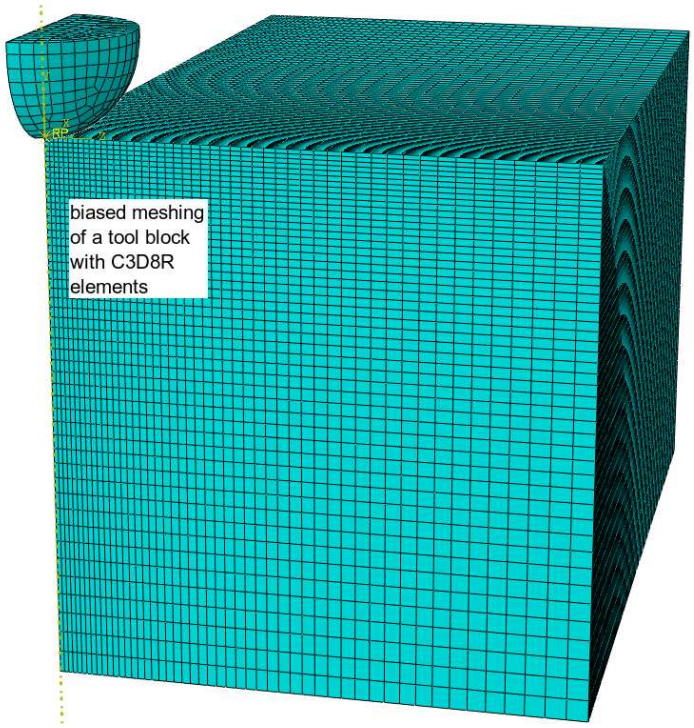

Figure 4.5: Biased meshing of a tool block with C3D8R linear brick elements and sand particle meshing scratch test model.

The contact between the sand particle and the block is assumed to be frictionless. This assumption was verified by comparing the numerical results to frictional contact, which were similar to the numerical results with frictionless contact [63]. Furthermore, adaptive meshing is enabled so that the severely deformed area is automatically

remeshed at specified frequencies. The adaptive meshing parameters are chosen optimally so that an accurate solution is obtained without significantly increasing the computational time.

4.2 Material Loss Due to Tool Wear

The scratch test results in surface deformation that is observed in the form of a groove developing along the path followed by the abrasive sand particle. Furthermore, the displaced groove material accumulates along the groove edges. The steps involved in modeling the scratch process and the resulting groove formation are shown in Figures 4.6 - 4.11 for two different particles sizes of 0.5 mm and 1.1 mm

In the first step, a frictionless contact is established between a spherical-shaped sand particle and the tool block surface, which is visible in Figures 4.6 & 4.7; the initial step of establishing frictionless contact between the sand particle and the tool block surface is shown for particles sizes 0.5 mm and 1.1 mm respectively.

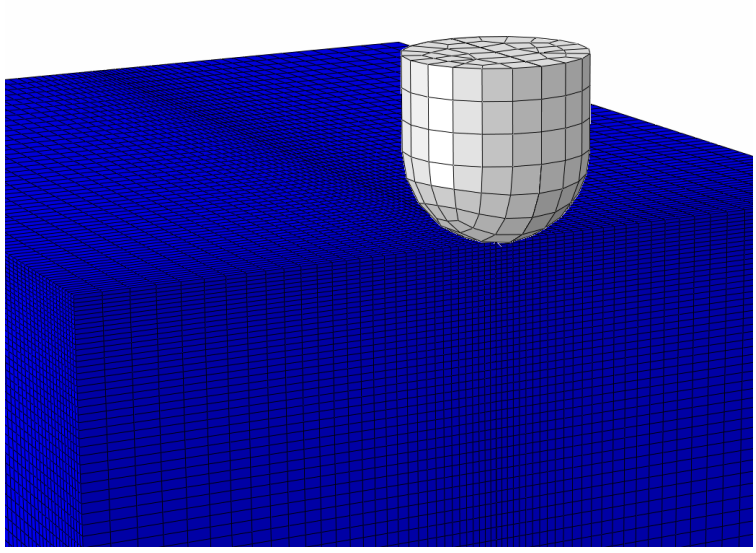

Figure 4.6: Frictionless contact is established between the sand particle and the tool block surface. Sand particle size is 0.5 mm.

Once contact is established, the sand particles are given a vertical displacement equal to the penetration depth. The resulting deformation is shown in Figure 4.8 for

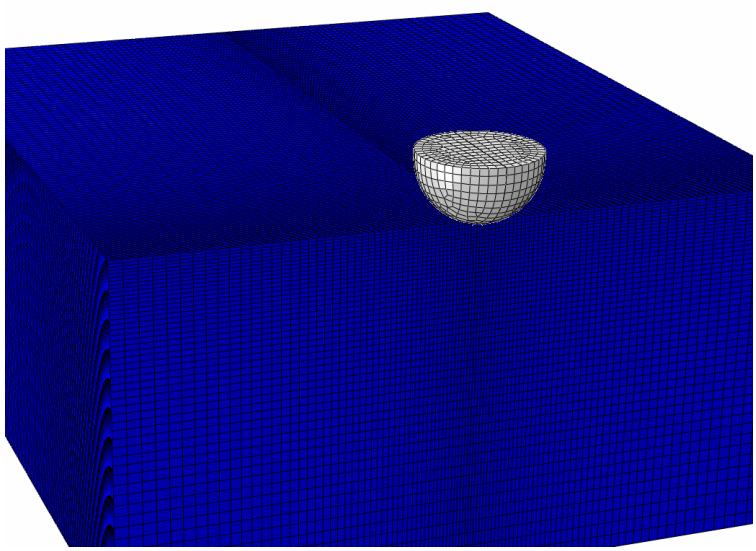

Figure 4.7: Frictionless contact is established between the sand particle and the tool block surface. Sand particle size is 1.1 mm.

the particle of size 0.5 mm The two subfigures show the particle-block system at the beginning of indentation and at the end. The deformation due to particle of size 1.1 mm is shown in Figure 4.9. The penetration depth in each case is one-tenth of the particle diameter.

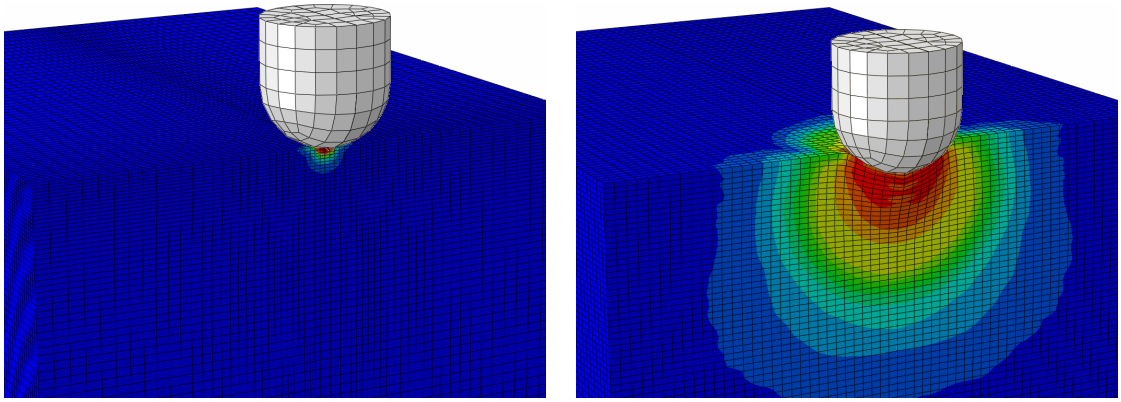

(a) (b)

Figure 4.8: A sand particle size of 0.5 mm that penetrates the tool block up to 0.05 mm, (a) at the beginning of the indentation (b) and at the end of indentation.

In Figures 4.10 and 4.11, where the scratching process begins and ends is shown

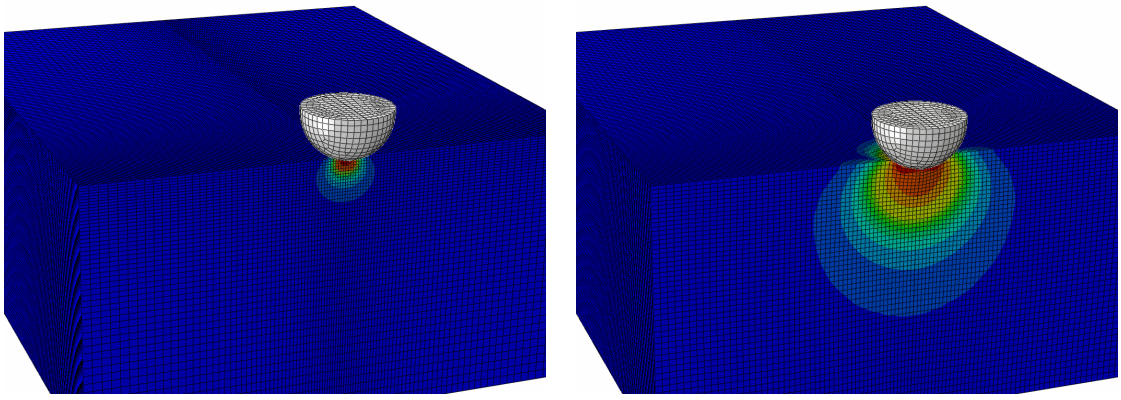

(a) (b)

Figure 4.9: A sand particle size of 1.1 mm that penetrates the tool block up to 0.11 mm (a) at the beginning of the indentation (b) at the end of indentation.

for the two particle sizes. In both cases, the scratch length is 1.25 mm.

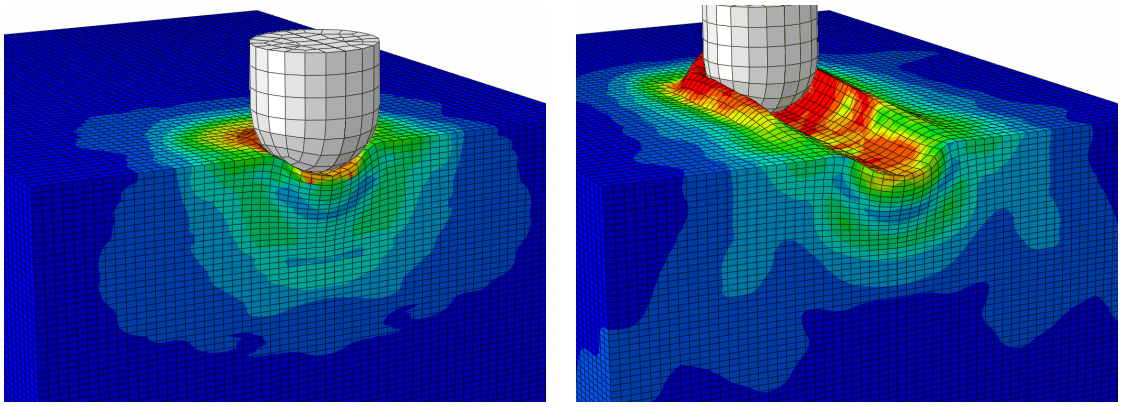

(a) (b)

Figure 4.10: A sand particle size of 0.5 mm that scratches the surface of tool block up to 1.25 mm (a) at the start of scratching (b) at the end of scratching.

The deformed blocks when the particles are withdrawn from contact are shown in Figures 4.12 & 4.13. This step is achieved by prescribing a displacement to the sand particles in the direction opposite of what is prescribed for indentation.

An enlarged view of the deformed tool block surface at the completion of the scratch process is shown in Figure 4.14 for the 0.5 mm particle. The deformed geometry indicates piling of the displaced groove material on the edges of the groove

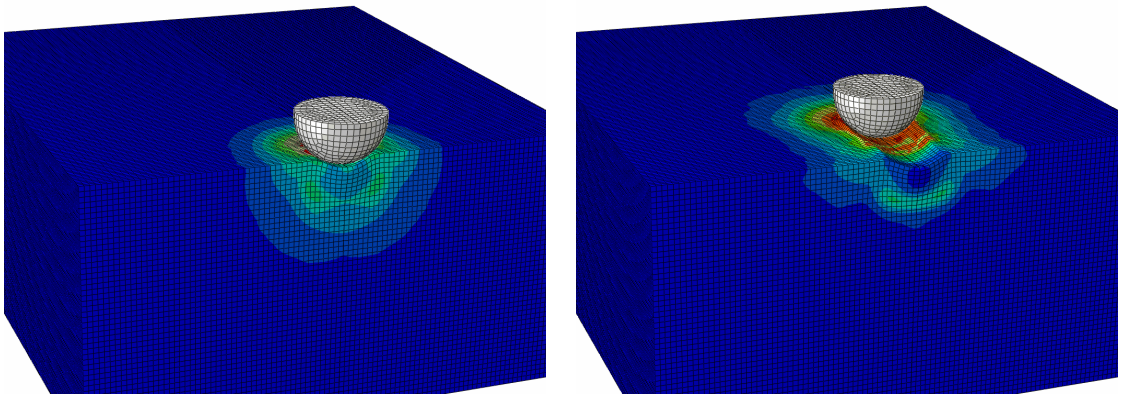

(a) (b)

Figure 4.11: A sand particle size of 1.1 mm that scratches the tool block up to 1.25 mm (a) at the start of scratching (b) at the end of scratching.

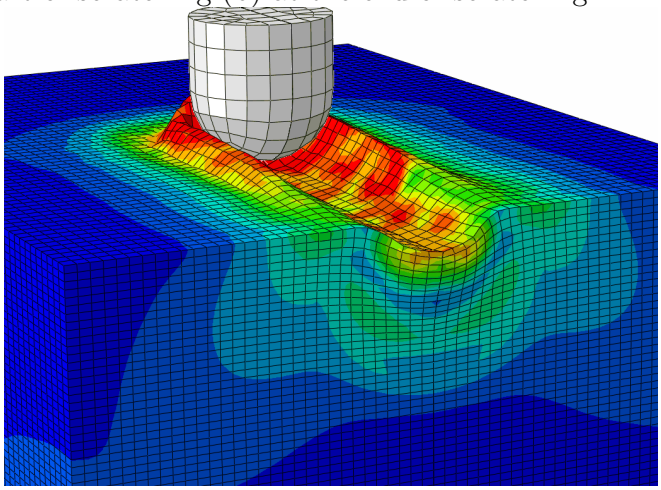

Figure 4.12: The contact between the sand particle and the tool block is removed as the particle moves away from the block surface. Sand particle size of 0.5 mm.

formed by the sliding sand particle. Similarly in Figure 4.15, the plastic deformations on the block surface can be seen when one of the very large sized sand particles (1.1 mm) has scratched the surface with a constant indentation depth of 0.11 mm.

A close-up of a front view of the cut section of the deformed tool surface, indicating the groove formation and the displaced groove material piling on its edges, is shown in Figure 4.16. This type of deformed surface geometry is important to measure the groove and the pile-up areas to determine wear loss as the difference in

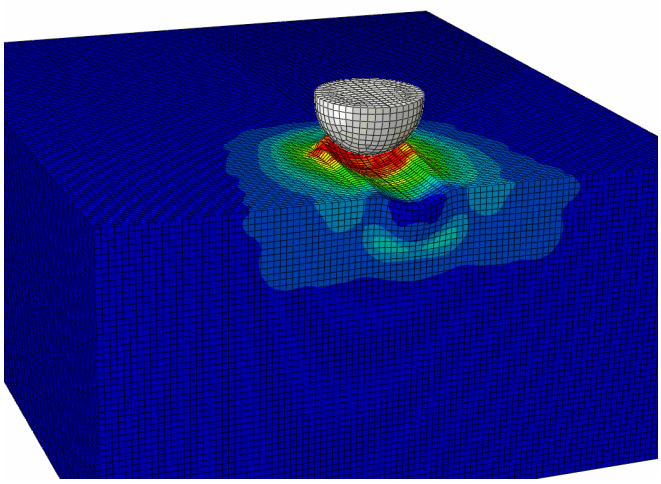

Figure 4.13: The contact between the sand particle and the tool block is removed as the particle moves away from the block surface. Sand particle size of 1.1 mm.

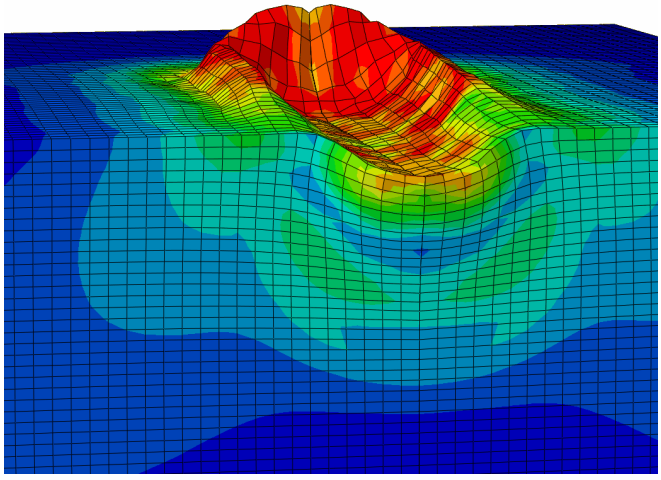

Figure 4.14: A magnified view of the deformed tool surface that shows groove formation and material pile-up on the groove edges with a sand particle size of 0.5 mm.

the displaced groove material volume and the pile-up material volume. The deformed surface geometry images are for two different categories of sand particles (i.e., large sand particle 0.5 mm and very large sand particle 1.1 mm).

The loss of material due to tool wear is calculated by using the concept of the material removal factor (f_{ab}) discussed in Chapter 2. Soil particles of various sizes are considered. Specifically, large sand particles with sizes 0.5 mm, 0.6 mm, 0.75 mm,

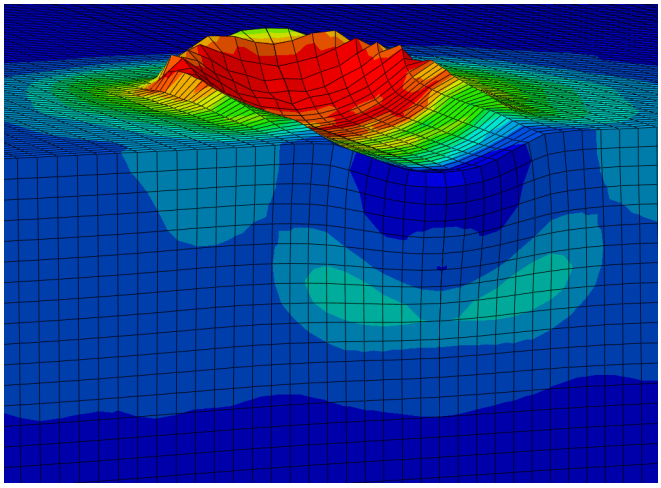

Figure 4.15: Figure shows that the permanent deformation is observed on the tool block with a sand particle size of 1.1 mm.

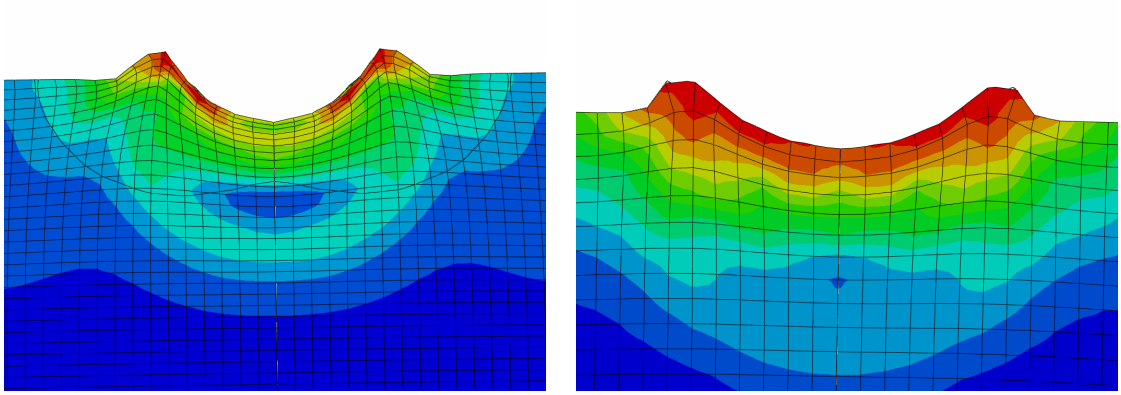

(a) (b)

Figure 4.16: A front view of the block section that shows permanent deformation (a) with a large sand particle size of 0.5 mm (b) with a very large sand particle size of 1.1 mm.

0.9 mm, and 1.0 mm and very large sand particles of sizes 1.1 mm, 1.3 mm, 1.5 mm, 1.7 mm, 1.9 mm, and 2.0 mm are considered.

Field tests suggest that the indentation depth on the tool surface is 10% of the sand particle size, but a comparative study with different indentation depths has also been included in this work.

In experimental studies, tool wear with a single sand particle scratching the tool

surface is measured using the following expression:

$$\frac{dm}{dt} = \rho \left(\frac{\pi y^2}{2} \right) \frac{dx}{dt} \tag{4.1}$$

where, $\frac{dm}{dt}$ is the mass loss rate in the scratching process, in gm/s, ρ is the density of a tool material, in $\frac{gm}{cm^3}$, y is penetration depth, in cm, $\frac{dx}{dt} = v(cos\alpha)$ is the relative speed of the particles with respect to the tool. In addition, $\alpha = 30^\circ$ is the angle of the tool with respect to the horizontal axis and v is the tillage speed (in cm/s).

When the sand particle size is 0.5 mm, the tillage speed is 3 km/h, and the indentation depth is 10% of the particle size, the above expressions lead to mass loss rate of approximately 0.00026 gm/s. In field tests where scratching is due to multiple particles, the tool material loss has been found to be approximately 0.006 $\pm$ 0.002 gm/s. Thus, on average, about 22 sand particles of size 0.5 mm. are needed to cause this wear rate. The multiparticle scratching is difficult to model with deterministic approaches. A combination of statistical and finite element methods may be needed to analyze the effect of multiparticle systems. Another approach may be the discrete element approach. In the present work, the focus is on the effect of individual particles scratching the tool surface.

To calculate the amount of wear loss due to a single particle, ZumGahr [10] expresses the volume of material lost as the product of the groove area (A_g) and the material removal factor (f_{ab}) (Equation 2.6). The factor f_{ab} is estimated using either the deformed surface geometry in numerical simulations or from experimental observations of the worn out tools. Here, the focus is on the former. For this reason, scratch test simulations were carried out to model the wear process and obtain estimates for groove and pile-up areas. The areas are calculated numerically using the nodal displacements measured from the deformed tool surface geometry. It is worth pointing out that in calculating the groove and pile-up areas, the displacement along

the scratch direction is ignored. The numerical results indicate that this displacement component is very small compared to the other two. The omission of it from area calculations makes the calculation of volumes displaced relatively simple.

Thus, the expression determining the tool wear is given by:

$$W_v = \rho f_{ab} A_g l \tag{4.2}$$

where, W_v is the amount of tool material lost with a single sand particle ρ is the density, l is the scratch distance, and A_g is the groove area.

From this, the rate of tool material lost during the tilling operation is derived as

$$\frac{dm}{dt} = \rho f_{ab} A_g v \tag{4.3}$$

where, $\frac{dm}{dt}$ is the tool wear loss, ρ is the density, f_{ab} is the material removal factor, A_g is the groove area in, and v is the sand particle speed (equivalent to the tilling speed of the tractor).

The numerical results, as shown in Figure 4.17, have been calculated using mathematical expressions that have been validated by Zum Gahr. The numerical results for the amount of tool material lost by a single soil particle scratching the block surface agree with the experimental results which can be used to determine the number of sand particles scratching the tool surface and to predict the total tool wear loss.

The total amount of tool material lost per second is calculated using the combined results of numerical studies and experimental analysis, and they are in the range of tool material lost during field tests.

In the next section, results from parametric studies conducted to understand the effects of indentation depth, particle size and tool speeds on material removal factor are discussed.

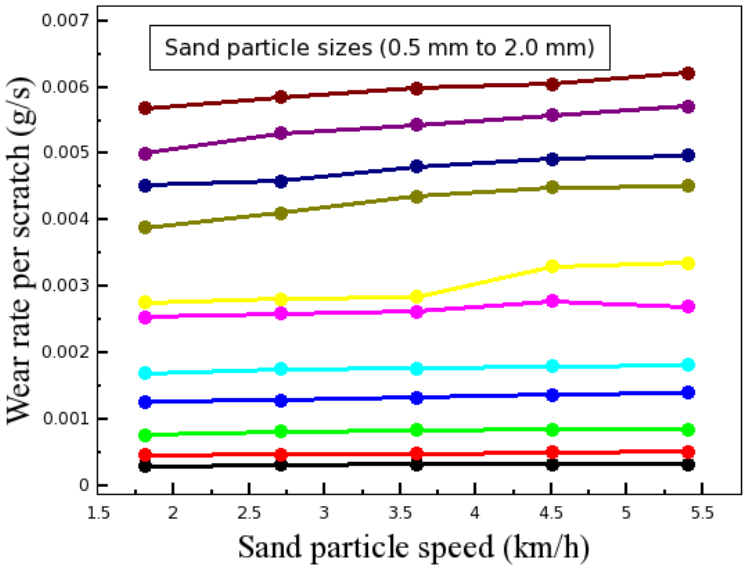

Figure 4.17: The amount of tool material loss with single sand particle sizes ranging from 0.5 mm to 2.0 mm with an approximate penetration depth (i.e., 10% of the particle size).

4.3 Parametric Study

4.3.1 Sand Particle Size

As discussed in Chapter 2, both microcutting and microploughing mechanisms are present when $0 < f_{ab} < 1$, and the microcutting mechanism is dominant with the increasing f_{ab} values. In soil tillage, tool wear depends on the soil particle sizes interacting with the tool surface. To investigate the effects of the soil particle size on the tool wear, the f_{ab} factor has been calculated using the finite element simulations.

In Figure 4.18, the f_{ab} factor is plotted against scratch distance for various sand particle sizes. The indentation/penetration depth for each of the cases is 0.1 mm. For each particle size, f_{ab} shows variation in the initial stage of the scratch process and then becomes a constant. This constant value increases with increasing particle size. It is interesting to note that for very large particle sizes, this factor has a value around 0.9 indicating that microcutting is significantly more dominant than microploughing. On the other hand, for smaller particle sizes, the material removal factor is around

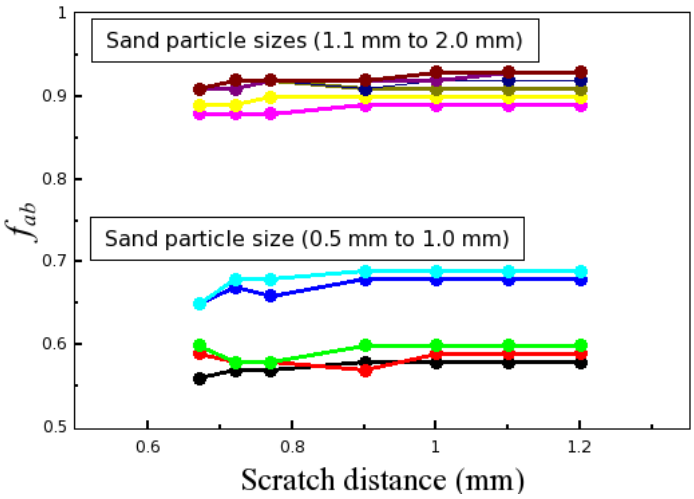

Figure 4.18: Variation of the material removal factor with the scratch distance for various particle sizes. Indentation depth = 10% of the particle size and tillage speed = 1.2 m/s.

0.55 to 0.7 indicating a significant presence of the microploughing mechanism as well.

In Figure 4.19, the variation of the "steady-state" value of f_{ab} is plotted against particle size. The depth of penetration is kept at 10% of the particle size in carrying out the numerical simulations. It is clear from the figure that the material removal factor, and hence the wear rate, go up with increasing particle size. While the increase is gradual in the range 0.5 mm to 1 mm and then, again, in the range 1 mm to 2 mm, there is a sharp increase in the material removal factor value at around a particle size of 1 mm. It is not clear why there is such a sharp change at this location, and further investigations are necessary to understand this jump. It is also interesting to note that when the sand particles are in the range of 0.5 mm to 1 mm, the material removal factor is in the range of 0.55 to 0.7 indicating that microploughing is less dominant but still contributes significantly to wear. However, for sand particle sizes in the range of 1 mm to 2 mm, the material removal factor has a value of 0.9 or higher indicating that microcutting plays a significant role in wear with microploughng playing a relatively minor role.

In field tests, the f_{ab} factor has been found to be approximately 0.7 which is

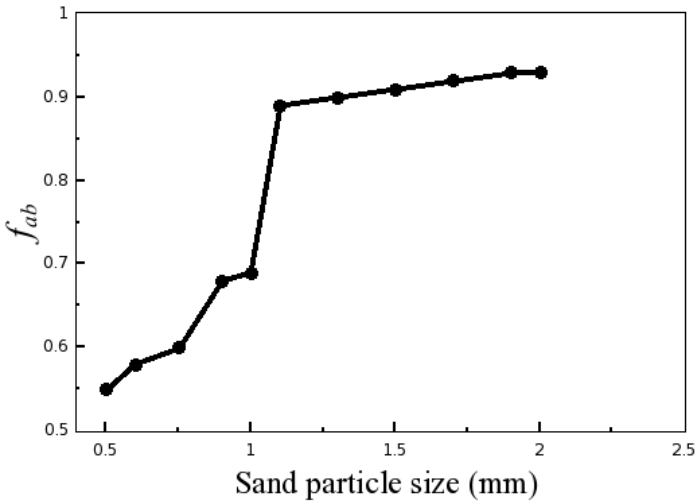

Figure 4.19: Variation of the material removal factor with various sand particle sizes.

comparable to the values found for large particle sizes in the numerical simulations.

4.3.2 Indentation Depth

During a tilling process, the contact between the soil particles and the tillage tool is complex with different particles indenting the tillage tool at the same or different speeds. Thus, the depth of indentation can be different for different particles. To understand the effect that the indendation depth has on the material removal factor, a parametric study has been carried out by varying the indentation depth for eight different particle sizes while keeping the tillage speed constant. The material removal factor is calculated from the finite element simulations and plotted against indentation depth for all of these particle sizes in Figure 4.20. It is interesting to note that the material removal factor does not vary appreciably with indentation depth for each particle size. The maximum change is about 10%.

It is important to keep in mind that even though the material removal factor does not change appreciably as the indentation depth is varied for a given particle size, the total material lost due to wear will increase since the amount of material displaced and the groove area both increase as the indentation depth increases.

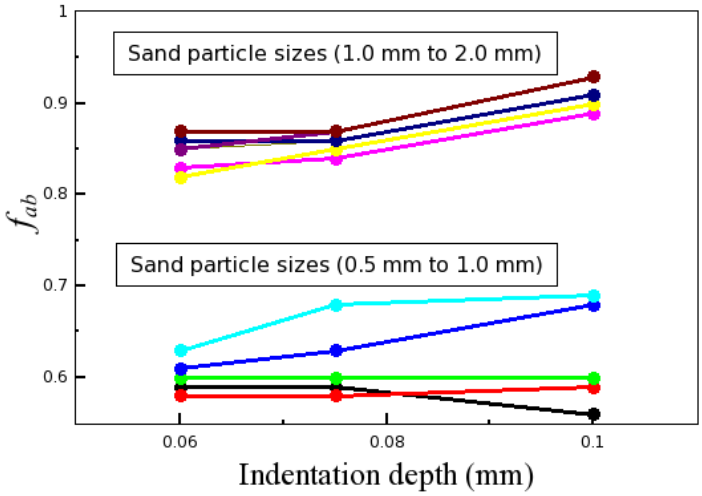

Figure 4.20: A plot showing the material removal factor for two different categories of sand particle sizes for three different depths of indentation.

4.3.3 Particle Speed

The dependence of the material removal factor (f_{ab}) on particle speed is shown in Figure 4.21. The particle size considered is 1.1 mm and the indentation depth is 0.1 mm. The speeds are varied from 1.8 km/h to 5.4 km/h. As the figure shows, the material removal factor shows a weak dependence on speed. The relative insensitivity of the material removal factor to particle speed can be attributed to the fact that the speeds considered are relatively low and therefore, the particle motion over the tool surface is essentially quasistatic. Since the material removal factor is close to 0.9, it can be concluded that for all of the speeds considered, microcutting contributes to almost all of the wear for this particle size and indent depth. Furthermore, for the speeds at which tractors operate during tilling, the wear rates are directly proportional to the tillage speeds.

4.4 Conclusions

The wear of tillage tools during tilling operations was studied using the two-body abrasion theory and the finite element method. Using a combination of the finite element method and analytical methods, the material removal factor was calculated

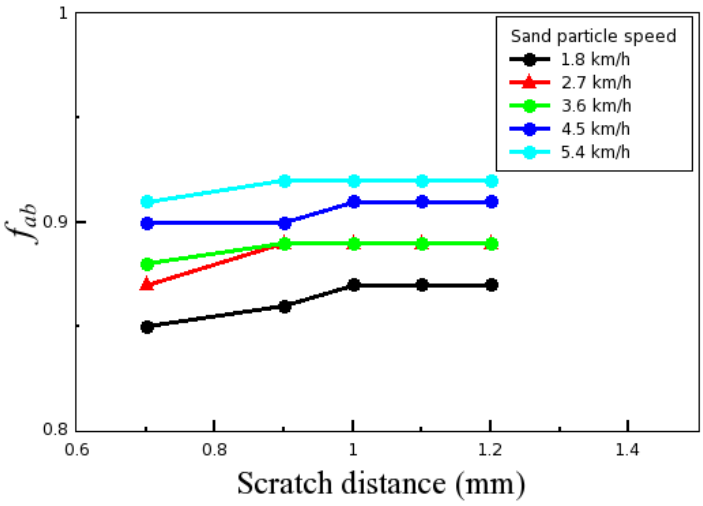

Figure 4.21: The effect of particle speed on the material removal factor. Sand particle size is 1.1 mm.

for various indentation depths of the soil particle, particle speeds over the tool surface and particle sizes. The numerical results indicate that the material removal factor is in the range of 0.55 to 0.7 for sand particle sizes in the range of 0.5 mm to 1 mm. These results are in agreement with experimental results where the material removal factor was found to be around 0.7. For larger sand particles, the material removal factor is much higher, around 0.9. Since the material removal factor values are higher than 0.5, it is clear that microcutting is the dominant mechanism in all cases. This mechanism becomes increasingly dominant as the particle size increases. Due to this, there is less volume of the material piling on the groove edges. Since the difference in the displaced material from the groove and the piled up area on the groove edges can be thought of as the amount of tool material lost due to wear induced by a single soil particle, it can be concluded that as the particle size increases, the wear rate given by Equation 4.3 increases.

The material removal factor does not appear to vary much as the particle speed is varied over values typically encountered in practice. The effect of indentation depth also has similar effects on the material removal factor. However, since the wear rates

are directly proportional to the displaced groove volume, it can be concluded that the wear rates increase with increasing indentation depth.

CHAPTER 5: SOIL TILLAGE - POWER REQUIREMENTS

The numerical studies discussed in the previous chapter were concerned with the wear of a tillage tool when a single soil particle scratches the tool surface. While these studies provide a valuable insight into the mechanisms involved in tool wear and the effect of various parameters on wear, they do not provide a means for studying the effect of tool wear on the power required for tillage operations. In order to understand the effect of tool wear on power requirements, simulations of the tilling process is necessary since the forces acting on the tillage tool are needed for power calculations. In this chapter, the soil-tool interaction problem is studied with the primary goal being to calculate the power needed for tilling operations using numerical simulations. The effect of toolwear on the power needed for tilling is not considered in the present study, although the additional effort needed is not very significant. A comment on studying the effect of tool wear is provided at the end of this chapter.

The tillage process involves three main steps: the initial contact of the tillage tool with soil, the penetration of the tool into the soil and the forward motion of the tool in the soil. In the present work, the first two steps are not considered and it is assumed that the tool is initially at the plowing depth [35, 41]. Contact between the tool and the soil is then established and the tool is given a prescribed velocity consistent with what is observed in practice. The soil upon contact with the tool begins to deform. The soil deformations are elastoplastic and large [36]. The soil material flows above, below and around the tool as the tool moves through the soil [32]. The main contributor to the power needed to move the tool depends on the thrust force (normal pressure) that the soil exerts on the tool [34]. Clearly, this force depends, to various degrees, on the plowing depth, tillage speed, soil properties and the tool-wear.

A survey of the literature on tool wear in tilling operations indicates a few attempts at modeling the tilling process using the finite element method [33,35]. Almost all of these attempts were based on an in-house code that used highly simplifying assumptions such as a predefined plane of separation during tilling, simple constitutive models and short lengths for tool movement (due to issues concerned with element distortion) [29].

In the present work, the tilling process is modeled using ABAQUS/Explicit which, as mentioned previously, is a robust nonlinear finite element software with built-in, sophisticated constitutive models for soil behavior and well-tested contact capabilities. The models are used to calculate the power consumption during plowing operations with different soil material parameters [51]. The numerical results are compared with experimental results which were provided by the tribology group at the School of Mines, National University of Colombia, Medellin, Colombia. In this chapter, these models, comparisons with experiments and the parametric studies carried out are discussed.

5.1 Geometry

The tillage operation is modelled as a two-dimensional, plane-strain problem where the soil is considered as a rectangular block of material and the plowing assembly (including the tool) is considered to be rigid. Numerical simulations carried out by assuming that the plowing assembly is deformable did not yield results that significantly differed from those of the rigid assembly. The assumption of a rigid assembly results in a significant decrease in the computational needed to run the analyses. For this reason, for all the analyses discussed in this section, the plowing assembly is considered to be rigid.

The soil block is taken to be 3 m in length and 0.6 m in height as shown in Figure 5.1. The plowing assembly geometry is based on the actual geometry of a typical plowing assembly as shown in Figure 5.2. In this figure, a CAD drawing of

an actual plowing assembly and the two-dimensional version of it are shown. The two-dimensional model along with the rectangular soil block is used in modeling the tilling process. It is worth pointing out that the finite element models previously considered by various researchers assume the tool to be a rectangular block. The model presented here is based on the actual tool geometry albeit two-dimensional.

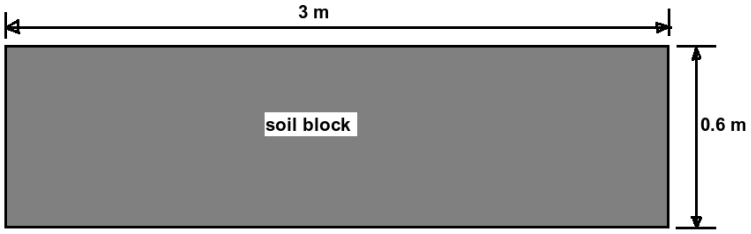

Figure 5.1: A 2D schematic of a soil block.

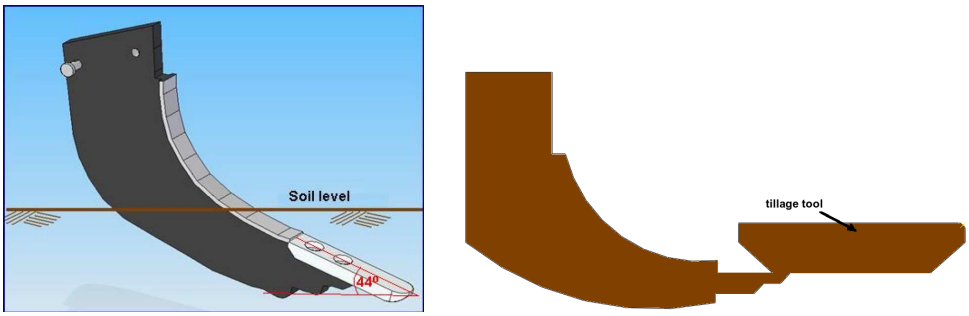

(a) (b)

Figure 5.2: Soil plowing assembly (a). A 3D model (b). A 2D model.

5.2 Constitutive Model

The mechanical behavior of soil is modeled using the Drucker-Prager Cap (DPC) plasticity model [37, 42]. DPC models are commonly used for describing the mechanical behavior of geological materials which are pressure-sensitive and undergo large deformations and compaction.To define the soil behavior using a cap plasticity model, the essential parameters required are soil friction and cohesion. In dry cohesionless soils, shear resistance is due to dry friction between the grains, and it is governed by the Coulomb law of friction.

The elastic behavior is taken to be linear and isotropic. The inelastic deformation is governed by the DPC model which consists of a shear failure surface, a cap and a smooth transition region from the shear failure region to the cap (see Figure 5.3). The cap is usually elliptical in shape and intersects the hydrostatic axis at a right angle.

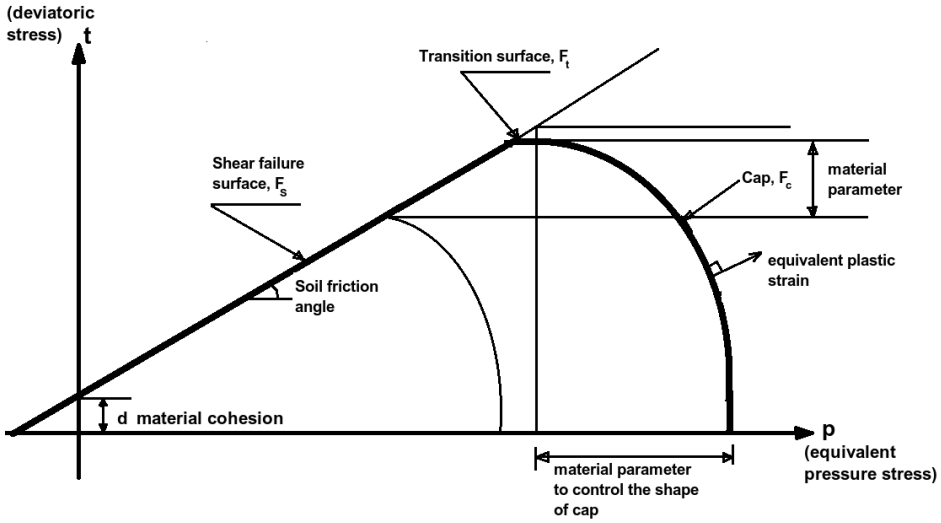

Figure 5.3: Cap plasticity model in the p-t plane.

The shear failure surface is defined by

$$F_s = t - p\tan\beta - d. \tag{5.1}$$

In this equation, β and d are the angle of friction of the material and cohesion, respectively. p is the negative of the hydrostatic stress defined by

$$p = -\frac{1}{3}\text{trace}\,(\sigma)$$

and t is a deviatoric stress measure defined by

$$t = \frac{1}{2}q\left[1 + \frac{1}{K} - \left(1 - \frac{1}{K}\right)\left(\frac{r}{q}\right)^3\right], \tag{5.2}$$

with q, the Mises equivalent stress, r the third stress invariant, and K is a material parameter equal to the ratio of the yield stress in triaxial tension to the yield stress in triaxial compression. In ABAQUS/Explicit, the value of K is always taken to be equal to unity.

The elliptical cap on the end of the Drucker-Prager shear failure model captures the effects of material compaction and dilatation. In the case of compaction, the cap surface provides hardening and bounds the yield surface in hydrostatic compression, whereas under dilatation, it provides softening as a function of increased volume when the material fails in shear. For example, the cap surface softens on volume increase when the plastic flow is on the shear failure yield surface and vice-versa when the plastic flow is on the cap surface.

$$F_c = \left[(p - p_a)^2 + \left(\frac{Rt}{1 + \alpha - \frac{\alpha}{cos\beta}} \right)^2 \right]^{1/2} - R(d + p_a tan\beta) = 0 \qquad (5.3)$$

where, R is a material parameter controlling the shape of the cap, α is a small number used for smooth transitioning from the shear failure to the cap surface, and p_a is an evolution parameter that is a function of the volumetric plastic strain and characterizes the hardening/softening behavior. This behavior is captured in ABAQUS by tabular data consisting of the mean effect stress p_b and the volumetric plastic strain.

The transition surface is given by:

$$F_t = \left((p - p_a)^2 + t - \left(1 - \frac{\alpha}{cos\beta} \right) (d + p_a tan\beta) \right)^{1/2} - \alpha(d + p_a tan\beta) = 0 \qquad (5.4)$$

The corresponding flow rule in the DPC model is as follows. For the cap surface, an associated flow rule, ie., the flow potential is the same as the yield surface, is used [62]. For the shear failure surface and the transition surface, a nonassociated

flow rule is used. Thus, in the cap segment, the flow potential is given by

$$G_c = \left[(p - p_a)^2 + \left(\frac{Rt}{1 + \alpha - \frac{\alpha}{cos\beta}} \right)^2 \right]^{1/2}$$

and the flow-potential in the shear failure and transition segments is given by

$$G_s = \left[(p - p_a \tan\beta)^2 + \left(\frac{t}{1 + \alpha - \frac{\alpha}{cos\beta}} \right)^2 \right]^{1/2}$$

It is important to note that the non-associative flow models lead to a non-symmetric stiffness matrices which in turn requires that an unsymmetric solver be used in the finite element simulations.

It is clear from the above that the parameters that are needed for full material description are E, ν, β, d, p_a, R, p_b and α. The values E, ν, β and d are given in Table 5.1 [52].

Table 5.1: Elasto-plastic properties of a sandy soil.

Elasto-plastic properties			
E	326200 Pa	d	350 Pa
ρ	1255.2 kg/m^3	β	57.8°

The cap hardening parameters p_a and p_b are given in Table 5.2 [52].

5.3 Load Step and Contact

The tillage process in the two-dimensional plane-strain setting is modelled in three load steps. The initial step establishes contact between the plowing assembly and the soil block (refer to Figure 5.4). This step is followed by a gravitational step, in which the soil block is subjected to gravitational load for 0.05 seconds, and the gravity effect is applied in the consecutive step.

Table 5.2: Cap hardening parameters used for modeling the soil deformation.

Cap hardening parameters					
σ_y (Pa)	ε^p	σ_y (Pa)	ε^p	σ_y (Pa)	ε^p
1	0	50000	0.110262	120000	0.185036
5000	0.014661	60000	0.125006	160000	0.208422
10000	0.028334	70000	0.138069	210000	0.228045
20000	0.053024	80000	0.149679	290000	0.248232
30000	0.074619	90000	0.160028	400000	0.266976
40000	0.093572	100000	0.16928	500000	0.280999

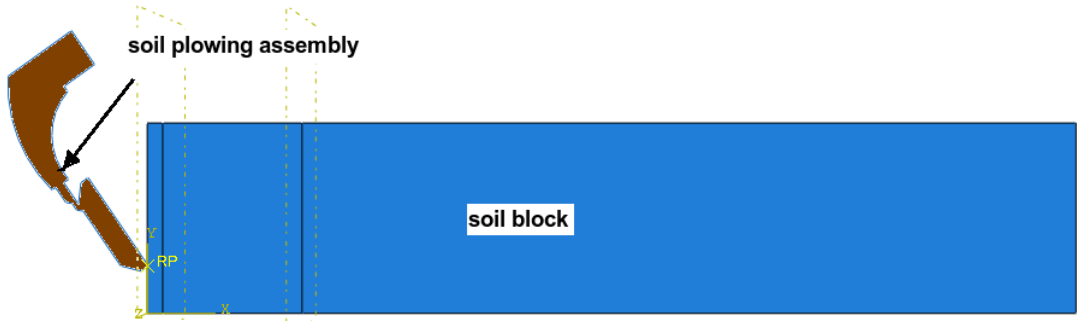

Figure 5.4: In the initial time step, contact is created between the rigid tool and the soil block.

In the third load step, the plowing assembly is given a constant speed to the right to simulate the tilling process. Contact conditions between soil and the tool assembly are defined appropriately. The friction between soil and the tool is modeled using Coulomb friction with a frictional coefficient of 0.2. Due to the large deformations involved, numerical problems due to element distortions are highly likely [25]. To overcome these issues, adaptive meshing is used in the soil block. The soil domain is remeshed in the contact areas frequently to avoid severely distorted elements. The speed of the tool assembly (tillage speed) is taken to be in the range of 3 km/h to 5 km/h, which are typical of what is seen during tilling operations.

To prevent the block from moving, a fixed boundary condition has been assigned to the bottom side of the soil block in all the steps. In the third load step, in addition to fixing the bottom edge, the right edge is also prevented from moving horizontally

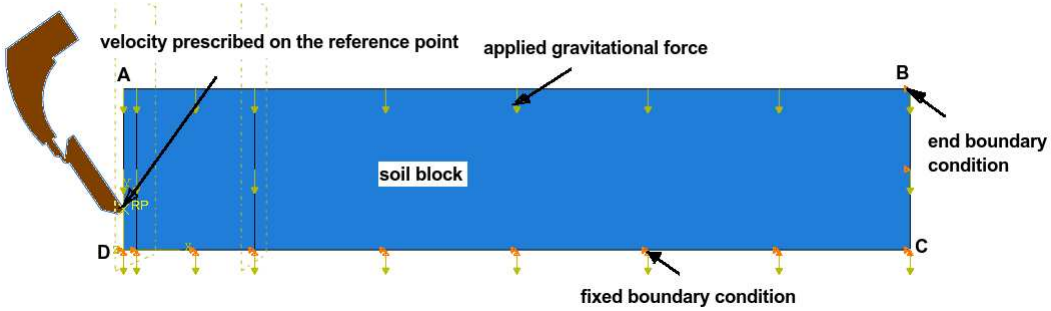

Figure 5.5: Boundary conditions used in the plane-strain tilling analyses.

as shown in Figure 5.5).

The soil block is meshed with four-noded, plane-strain quadrilateral elements with reduced integration (CPE4R). The block is discretized with 39,000 elements, as shown in Figure 5.6. A biased meshing technique is used to generate a fine mesh near the soil-tool interface and a coarse mesh away from the interface where the deformations are not as severe.

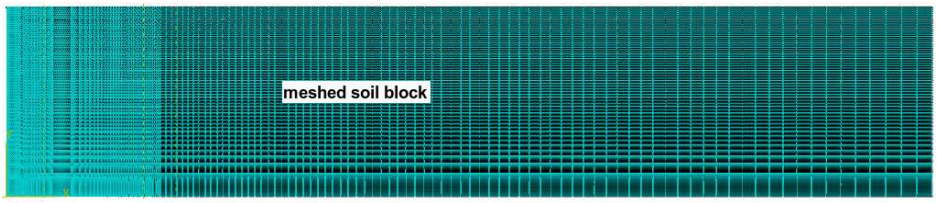

Figure 5.6: Biased meshing of a soil block with 39,000 CPE4R elements.

Simulations were carried out with a higher number of elements as well. The results from these finer mesh studies were not significantly different from those obtained with 39,000 elements. Therefore, the total number of elements considered are 39,000 in all the numerical studies discussed in this section.

5.4 Results

The results from the numerical simulations of the tilling process are discussed in this section. The nature of the soil deformation during tilling is studied and the power needed to carry out tilling operations is studied as various tilling parameters

are varied.

In the first step, the gravitational load is applied on the soil block. The resulting deformation of the block is shown in Figure 5.7. In this figure, only the left part of the block is shown to highlight the nature of the deformations due to gravity. The contours in the figure represent Mises stress levels with red being the highest. The shape shown is also the deformed configuration. Clearly, gravitational loading does cause significant deformation as expected.

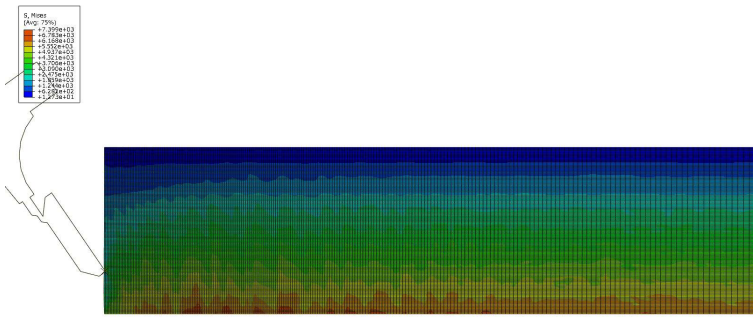

Figure 5.7: An enlarged view of a section of the soil block subjected to gravitational loading prior to tilling.

Following the gravitational loading, the rigid plowing assembly is moved against the soil block in the horizontal direction at a speed of 3.6 km/h and a plowing depth of 0.3 m. The deformed shape and the contours for the corresponding Mises stresses are shown in Figure 5.8. The deformed shape and the corresponding Mises stresses when a ploughing distance of 1 m is reached are shown in Figure 5.9. It is interesting to note the nature of the deformation. As tilling continues, soil piles up on top of the tool and then flows over it. It is also worth noting that, due to adaptive meshing, the element distortions are not very significant.

The stress that the soil exerts on the tool as the soil moves over it is the stress that the tool has to overcome for motion in the soil. This will be discussed further in the next section. It is interesting to note that the tool is able to travel through the soil block for well over a length of 1 m. without any numerical errors. This is

Figure 5.8: Soil deformation when the tool has traveled approximately 10 cm along the length of the soil block.

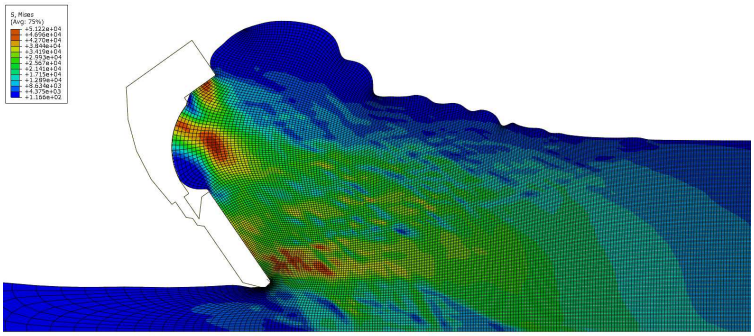

Figure 5.9: Soil deformation observed when the tool has traveled for a distance of 1 m.

one aspect that distinguishes the present study from the previous studies reported in the literature, where the numerical errors due to severe element distortions appeared to prevent the tools from moving into the soil for significant distances. Another aspect that sets this study apart from previous studies is that no specific plane for material separation had to be specified a priori and planes defining failure planes for soil deformation are not necessary.

5.5 Power Calculations

The stress that the soil exerts on the tool surface can be used to calculate the power consumed in tilling operations. The power is calculated by multiplying the horizontal component of the traction vector on the tool surface with the tool speed and integrating over the entire tool surface. In Figure 5.10, the power is plotted against time for a tillage speed of 1 m/s. The initial sharp rise corresponds to the

initial unsteady process. Once steady-state conditions are established, the power required for tilling becomes essentially constant as the figure shows.

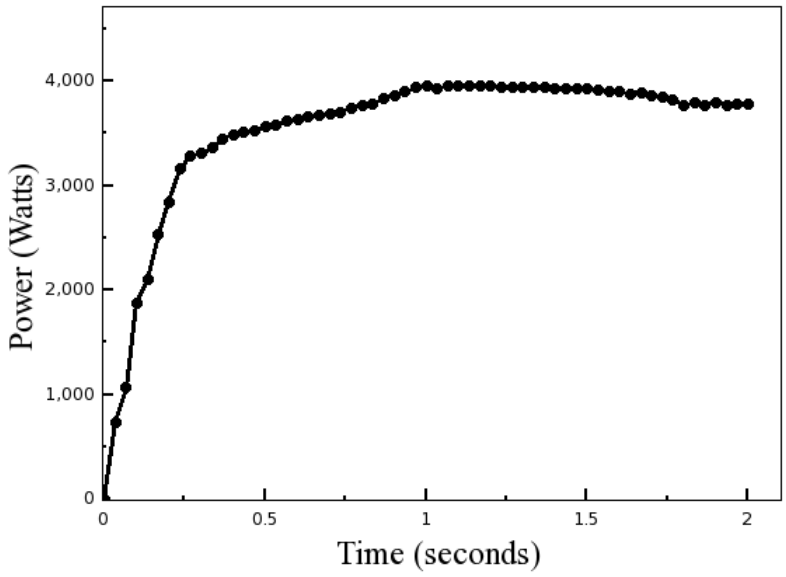

Figure 5.10: Variation of power needed for tilling with time.

The dependence of the power needed for tilling on tillage speed is studied by carrying out numerical simulations for various tillage speeds ranging from 2.0 km/h to 4 km/h (approximately 0.5 m/s to 1 m/s). The power needed for tilling is plotted against tool speed in Figure 5.11. In all the cases, the plowing depth is taken to be 300 mm. For comparison purposes, experimental results are shown in the figure. It is clear from the figures that the difference between the experimental and numerical results is significant at lower speeds. At high speeds, the difference is somewhat smaller. The discrepancies between the numerical and experimental results are likely due to the assumption of plane-strain model in the numerical simulations, the constitutive model used for the mechanical response of soil and other uncertainties associated with modeling the problem accurately. Nevertheless, the numerical results qualitatively agree with the experimental results: the power needed for tilling monotonically increases with tillage speed. It is also interesting to note that the dependence on the tool speed is essentially linear.

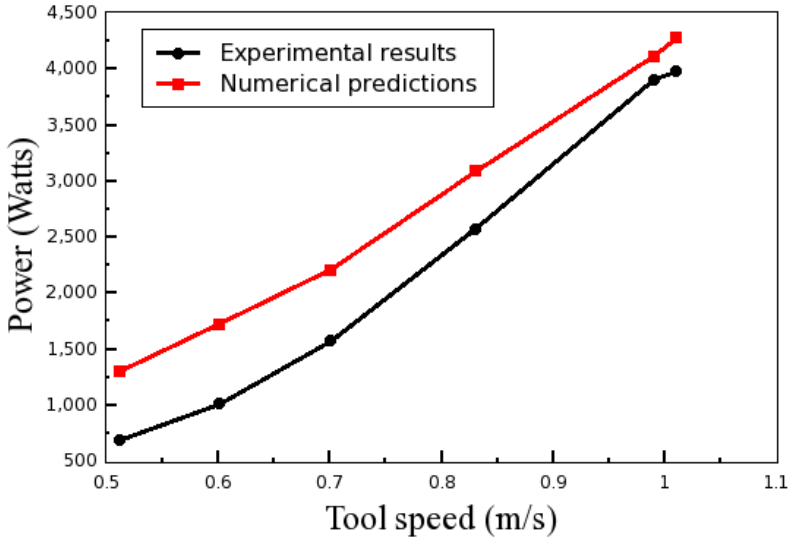

Figure 5.11: A comparison of the power consumed for different tractor speeds.

The power needed for tilling depends on the moisture content in the soil. In order to investigate the effect of moisture content on power, the moisture content is varied. Using the expressions readily available in the literature, the corresponding material parameters in the Drucker-Prager model are calculated, and numerical simulations were carried out. The power values are calculated for various values of moisture content and plotted against moisture content in Figure 5.12. For comparison purposes, experimental values are also shown. It is interesting to note that the agreement between the two curves is reasonably good initially whereas for larger moisture content values, the agreement diverges. However, as before, the numerical results qualitatively agree with the experimental values. Of particular note is that both the experimental and numerical values show a sharp drop in the power needed at around 30% moisture content. As mentioned before, the simplifying assumptions made in the models contribute to these differences.

The plowing depth is another important parameter that affects tool wear rates and power consumption. In Figure 5.13, the power required for tilling is plotted against plowing depth. The tillage speed is taken to be 1.2 m/s. As the depth

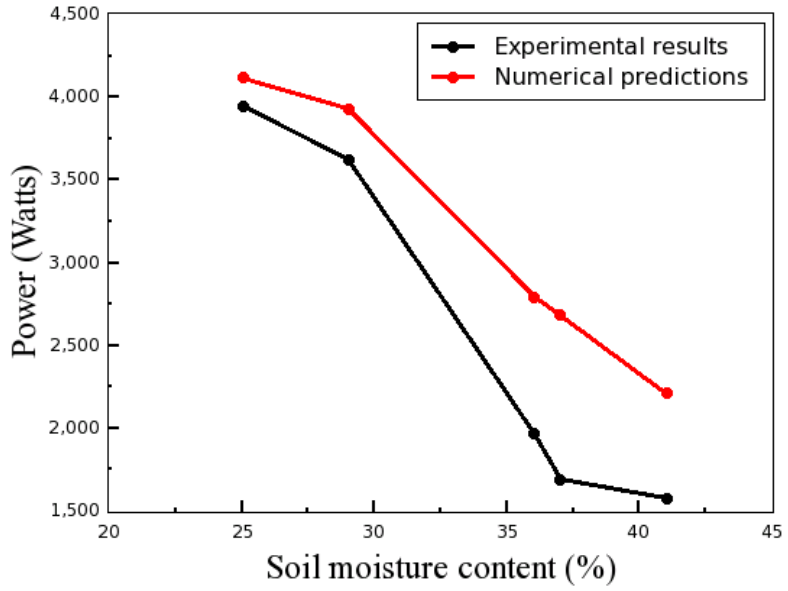

Figure 5.12: A comparison of power needs predicted numerically and experimentally, showing the effects of soil moisture content.

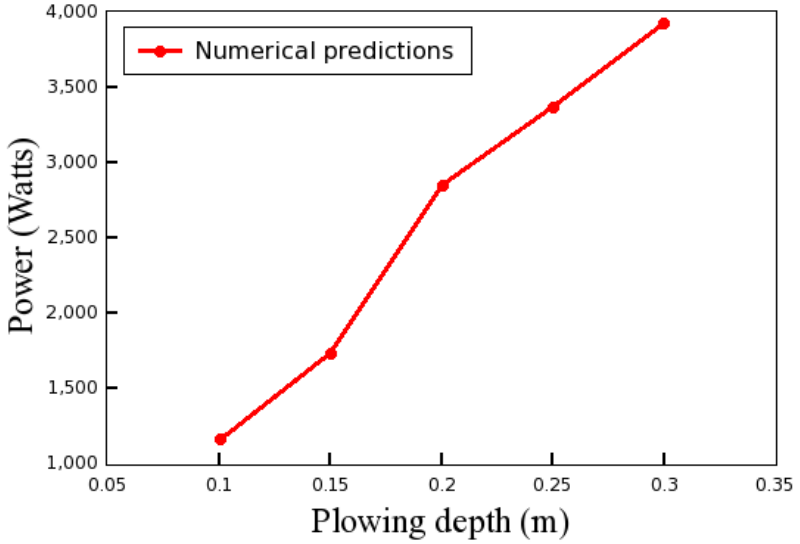

Figure 5.13: A plot showing the effects of varying plowing depth in terms of power requirements calculated numerically.

increases, the power needed also increases, as expected. It is interesting to note again that the increase is almost linear for the values of the depths considered.

5.6 Conclusions

In this chapter, results from numerical simulations of the tilling process were discussed. The simulations assumed a plane-strain model for tilling with a rigid plowing assembly. The objectives of these simulations were to understand the effect of tool speed, plowing depth and soil type on power consumption.

The numerical predictions of power consumed during tilling agree with experiments qualitatively (i.e., show similar trends). However, quantitative agreements are good for some combinations of the tillage parameters and substantially worse for other combinations of these parameters. The reasons for the differences in the numerical results and experimental results are likely due to the plane-strain assumption, large uncertainties in material parameters and the assumption to model a sand instead of the actual soil.

The numerical results indicate that the power required for tilling increases with plowing depth and tillage speed. The dependence of power consumption on the plowing depth and tillage speed appears to be linear. As the moisture content of the soil increases, the power consumption decreases. An interesting observation is that the drop in power consumption is dramatic as soon as a "critical" value for moisture content is reached.

The focus in this chapter was on calculating the power required in a tilling operation. The effect of a worn-out tool on the power consumption was not studied. An interesting study would be to replace the tool in the simulations by a worn-out tool and carry out the numerical simulations. Such a study would be beneficial in understanding the effect of tool-wear on tilling quality and power consumption.

CHAPTER 6: CONCLUSIONS

Tillage tool wear is the primary reason for increased downtimes of farm equipment and energy consumption during tilling. Many variables affect tool wear, and it is nearly impossible to conduct a comprehensive experimental study on the effect of these variables on tool wear. In this work, the viability of the finite element method as a tool for conducting virtual experiments to understand tool wear and predict power requirements was investigated. The numerical experiments were conducted using the commercial finite element software ABAQUS/Explicit.

Tool wear simulations were carried out using two-body abrasion models, where the soil particle was assumed to slide on a flat tillage tool surface at a prescribed speed. The classical plowing theory along with the concept of material removal factor was used to quantify material losses in the tool due to wear. The numerical prediction of the material removal factor was found to be in reasonable agreement with the experimental results. Following the validation with the numerical results, numerical studies were carried out to study the effect of various parameters such as the tool speed, tillage depth and soil particle size. In all of the studies, the material removal factor was well above 0.5 indicating that the dominant wear mechanism is microcutting. The numerical results also show that the wear losses are the highest for sand particles of size greater than 0.5 mm. Increased tool speed also increases wear rates which is consistent with experimental observations.

In addition to tool wear studies, numerical simulations were also carried out to study tool interaction with soil in a two-dimensional setting. The soil deformation during tool movement was assumed to be plane-strain. The Drucker-Prager constitutive model was used to describe the mechanical behavior of the soil. The primary

purpose of this study was to predict power requirements during tilling operations as tilling speed, plowing depth and soil type were varied. The numerical results agree qualitatively with the experimental results. The differences are most likely due to the assumption of two-dimensional plane-strain deformations and the assumption to model deformations in sand (and the numerical values used in the constitutive parameters) used for the soil. Nevertheless, the qualitative agreements show that the parametric studies are still useful for an understanding of the effect of various tillage parameters on power consumption.

The present work advances the application of the finite element method to study tillage tool wear in a significant way. The study brings together state-of-the-art finite element technologies and wear theories to understand wear mechanisms in tillage tools. It demonstrates the viability of using finite element simulations as virtual experiments and for optimizing tillage parameters for longer tool life. However, further refinements to the models are needed to reliably use simulations for tool design and for predicting power requirements.

Recommendations for future work are as follows. During the soil-tool interaction, the soil particles of different shapes typically slide and rotate and these shapes can affect the tool wear rates. In addition, when a soil particle scratches the virgin tool surface, the tool surface in the worn area can have a mechanical behavior different from the virgin surface. The cumulative effect of multiple particles scratching the surface needs to be accounted for in a statistical sense. Additionally, the constitutive behavior of the tool needs to include thermal effects since frictional effects and large deformations create significant localized heating. The power consumption and wear predictions too can be improved by considering three-dimensional models along with more sophisticated constitutive models for soil that take into account the heterogeneity of the soil.

REFERENCES

[1] E. Rabinowicz, L. A. Dunn, P. G. Russel, *A study of abrasive wear under three-body conditions* Wear 4 (1961) 345-355.

[2] T. O. Mulhearn, L. E. Samuels, *The Abrasion of Metals: A model of the process* Wear 5 (1962) 478-498.

[3] R. C. D. Richardson, *The wear of metallic materials by soil-practical phenomena* Journal for Agricultural Engineering Research 12 (1967) 22-39.

[4] W. R. Gill, G. E. V. Berg, *Soil dynamics in tillage and traction* Agricultural Research Science, United States Department of Agriculture, U.S. Government Printing Office, Washington, D.C. 20402 (January 1968).

[5] M. A. Moore, *Abrasive wear by soil* Tribology International (1975) 105-110.

[6] A. A. Torrence, *A new approach to the mechanics of abrasion* Wear 67 (1981) 233-257.

[7] A. A. Torrence, *The Correlation of Abrasive Wear Tests* Wear 63 (1980) 359-370.

[8] K. Z. Gahr, *Formation of wear debris by the abrasion of ductile materials* Wear 74 (1982) 353-373.

[9] W. M. Garrison Jr., R. A. Garriga, *Ductility and the Abrasive Wear of an Ultrahigh Strength Steel* Wear 85 (1983) 347-360.

[10] K. Z. Gahr, *Tribology Series 10 - Microstructure and Wear of Materials* Elsevier Science Publishing Company Inc., 52, Vanderbilt Avenue, New York, NY 10017.

[11] W. M. Garrison Jr., *Abrasive Wear Resistance: The effects of ploughing and the removal of ploughed material* Wear 114 (1987) 239-247.

[12] K. Z. Gahr, *Modelling of Two-Body Abrasive Wear* Wear 124 (1988) 87-103.

[13] A. G. Wang, I. M. Hutchings, *Mechanisms of Abrasive Wear in a Boronized Alloy Steel* Wear 124 (1988) 149-163.

[14] S. Jacobson, P. Wallen, S. Hogmark, *Fundamental aspects of abrasive wear studied by a new numerical simulation model* Wear 123 (1988) 207-223.

[15] A. G. Wang, I. M. Hutchings, *The Number of Particle Contacts in Two-Body Abrasive Wear of Metals by coated abrasive papers* Wear 129 (1989) 23-35.

[16] I. M. Hutchings, *Tribology: Friction and wear of Engineering Materials* CRC Press, Inc., 2000 Corporate Blvd., N.W., Boca Raton, Florida, 33431.

[17] J. A. Williams, Y. Xie, *The generation of wear surfaces by the interaction of parallel grooves* Wear 155 (1992) 363-379.

[18] J. M. Fielke, T. W. Riley, G. Slattery, R. W. Fitzpatrick, *Comparison of tillage forces and wear rates of pressed and cast cultivator shares* Journal of Agricultural Engineering 25 (1993) 317-328.

[19] T. A. Adler, R. P. Walters, *Wear and scratch hardness of 304 stainless steel investigated with a single scratch test* Wear, 162-164 (1993) 713-720.

[20] K. Terzaghi, R. B. Peck, G. Mesri, *Soil mechanics in engineering practice* John Wiley & Sons, Inc., New York, USA (3rd edition) 1995.

[21] L. Borgesson, O. Karnland, L-E. Johannesson, *Modelling of the physical behavior of clay barriers close to water saturation* Engineering Geology 41 (1996) 127-144.

[22] B. K. Prasad, S. Das, A. K. Jha, O. P. Modi, R. Dasgupta, *Factors controlling the abrasive wear response of a zinc-based alloy silicon carbide particle composite* Composites Part A 28A (1997) 301-308.

[23] Z. Owsiak, *Wear of symmetrical wedge-shaped tillage tools* Soil & Tillage Research 43 (1997) 295-308.

[24] M. G. Hamblin, G. W. Stachowiak, *Characterisation of surface abrasivity and its relation to two-body abrasive wear* Wear 206 (1997) 69-75.

[25] G. Oettl, R. F. Stark, G. Hofstetter, *A comparison of elasticplastic soil models for 2D FE analyses of tunnelling* Computers and Geotechnics 23 (1998) 19-38.

[26] J. Jiang, F. Sheng, F. Ren, *Modelling of two-body abrasive wear under multiple contact conditions* Wear 217 (1998) 35-45.

[27] R. L. Kushwaha, Z. X. Zhang, *Evaluation of factors and current approaches related to computerized design of tillage tools: A review* Journal of Terramechanics 35 (1998) 69-86.

[28] J. Shen, R. L. Kushwaha, *Soil-Machine Interaction - A Finte Element Perspective* Marcel Dekker, Inc., 270 Madison Avenue, New York, New York 10016 (1998).

[29] A. M. Mouazen, M. Nemenyi, *A review of the finite element modeling techniques of soil tillage* Mathematics and Computers in Simulation 48 (1998) 23-32.

[30] R. Gahlin, S. Jacobson, *The particle size effect in abrasion studied by controlled abrasive surfaces* Wear 224 (1999) 118-125.

[31] J. M. Fielke, *Finite Element Modelling of the Interaction of the Cutting Edge of Tillage Implements with Soil* Journal for Agricultural Engineering Research 74 (1999) 91-101.

[32] U. A. Rosa, D. Wulfsohn, *Constitutive model for high speed tillage using narrow tools* Journal of Terramechanics 36 (1999) 221-234.

[33] A. M. Mouazen, M. Nemenyi, *Finite element analysis of subsoiler cutting in non-homogeneous sandy loam soil* Soil & Tillage Research 51 (1999) 1-15.

[34] A. M. Mouazen, M. Nemenyi, *Tillage Tool Design by the Finite Element Method: Part 1. Finite Element Modelling of Soil Plastic Behavior* Journal for Agricultural Engineering Research 72(1999) 37-51.

[35] A. M. Mouazen, M. Nemenyi, H. Schwanghart, M. Rempfer, *Tillage Tool Design by the Finite Element Method: Part 2. Experimental Validation of the Finite Element Results with Soil Bin Test* Journal for Agricultural Engineering Research 72 (1999) 53-58.

[36] A. M. Mouazen, M. Nemenyi, *Finite element modelling of subsoiling processes* Advances in GeoEcology 32 (2000) 126-134.

[37] C. S. Desai, *Mechanics of materials and interfaces: the disturbed state concept* [electronic resource] Boca Raton, FL:CRC Press, 2001.

[38] L. Fang, J. Xing, W. Liu, Q. Xue, G. Wu, X. Zhang, *Computer simulation of two-body abrasion processes* Wear 251 (2001) 1356-1360.

[39] J. L. Bucaille, E. Felder, G. Hochstetter, *Mechanical analysis of the scratch test on elastic and perfectly plastic materials with the three-dimensional finite element modelling* Wear 249 (2001) 422-432.

[40] A.M.Mouazen, H. Ramon, *A numerical-statistical hybrid modeling scheme for evaluation of draught requirements of subsoiler cutting a sandy loam soil, as affected by moisture content, bulk density and depth* Soil & Tillage Research 63 (2002) 155-165.

[41] A. M. Mouazen, H. Ramon, Josse De Baerdemaeker, *Effects of bulk density and moisture content on selected mechanical properties of sandy loam soil*, Biosystems Engineering (2002) 83(2) 217-224.

[42] R. O. Davis, A. P. S. Selvadurai, *Plasticity and Geomechanics* Cambridge University Press, The Edinburgh Building, Cambridge, CB@ 2RU, UK, (2002).

[43] A. A. Torrence, *The effect of grit size and asperity blunting on abrasive wear* Wear 253 (2002) 813-819.

[44] N. H. Abu-Hamdeh, R. C. Reeder, *A nonlinear 3D finite element analysis of the soil forces acting on a disk plow* Soil & Tillage Research 74 (2003) 115-124.

[45] M. Abo-Elnor, R. Hamilton, J. T. Boyle, *3D Dynamic analysis of soil-tool interaction using the finite element method* Journal of Terramechanics 40 (2003) 51-62.

[46] S. R. Ashrafizadeh, R. L. Kushwaha, *Soil failure model in front of a tillage tool action- a review* The Canadian society for engineering in agricultural, food and biological systems meeting 2003, Montreal, Quebec, July 6-9, 2003.

[47] M. Barge, G. Kermouche, P. Gilles, J. M. Bergheau, *Experimental and numerical study of the ploughing part of abrasive wear* Wear 255 (2003) 30-37

[48] M. Abo-Elnor, R. Hamilton, J. T. Boyle, *Simulation of soil blade interaction for sandy soil using advanced 3D finite element analysis* Soil & Tillage Research 75 (2004) 61-73.

[49] L. Fang, Q. Cen, K. Sun, *An Explanation for Abrasive Critical Size Effect in Two-Body Abrasion by 3D FEM and Monte-Carlo Simulation* Computational Mechanics, WCCM VI in conjunction with APCOM'04, Sept. 5-10, 2004, Beijing, China.

[50] L. Fang, Q. Cen, K. Sun, W. Liu, X. Zhang, Z. Huang, *FEM computation of groove ridge and Monte Carlo simulation in two-body abrasive wear* Wear 258 (2005) 265-274.

[51] S. Y. Ibarra, E. McKyes, R. S. Broughton, *A model of stress distribution and cracking in cohesive soils produced by simple tillage implements* Journal of Terramechanics 42 (2005) 115-139.

[52] R. C. Chiroux, W. A. Foster Jr., C. E. Johnson, S. A. Shoop, R. L. Raper, *Three-dimensional finite element analysis of soil interaction with a rigid wheel* Applied Mathematics and Computation 162 (2005) 707-722.

[53] A. A. Torrence, *Modelling abrasive wear* Wear 258 (2005) 281-293.

[54] Y. Bayhan, *Reduction of wear via hardfacing of chisel ploughshare* Tribology International 39 (2006) 570-574.

[55] R. Jafari, T. T. Hashjin, S. Minaee, M. H. Raoufat, *Large deformation modeling in soil-tool interaction using advanced 3D nonlinear finite element approach* Proceedings of the 6th WSEAS International Conference on Simulation, Modelling and Optimization, Lisbon, Portugal. September 22-24, 2006.

[56] U Er, B. Par, *Wear of plowshare components in SAE 950C steel surface hardened by powder boriding* Wear 261 (2006) 251-255.

[57] I. Sevim, I. B. Eryurek, *Effect of abrasive particle size on wear resistance in steels* Materials and Design 27 (2006) 173-181.

[58] A. Zmitrowicz, *Wear patterns and laws of wear* Journal of Theoretical and Applied Mechanics 44 (2006) 219-253.

[59] A. K. Bhakat, A. K. Mishra, N. S. Mishra, *Characterization of wear and metallurgical properties for development of agricultural grade steel suitable in specific soil conditions* Wear 263 (2007) 228-233.

[60] R. J. Godwin, *A review of the effect of implement geometry on soil failure and implement forces* Soil & Tillage Research 97 (2007) 331-340.

[61] T. Fouda, M. El-Tarhuny, *A study of ploughshares wearing behavior under conditions of sandy loam soil* Journal for Agricultural Engineering 24(4) (2007) 831-848.

[62] S. Helawany, *Applied Soil Mechanics with Abaqus Applications* John Wiley & Sons, Inc., New Jersey, c2007.

[63] S. C. Bellemare, M. Dao, S. Suresh, *Effect of mechanical properties and surface friction on elasto-plastic sliding contact* Mechanics of Materials 40 (2008) 206-219.

[64] S. Davoudi, R. Alimardani, A. Keyhani and R. Atarnejad, *A two dimensional finite element analysis of a plane tillage tool in soil using a non-linear elasto-plastic model* American-Eurasian Journal for Agriculture & Environment Science, 3 (3): (2008) 498-505.

[65] Z. Horvat, D. Filipovic, S. Kosutic, R. Emert, *Reduction of mouldboard plough share wear by a combination technique of hardfacing* Tribology International 41 (2008) 778-782.

[66] A. Natsis, G. Petropoulos, C. Pandazaras, *Influence of local soil conditions on mouldboard ploughshare abrasive wear* Tribology International 41 (2008) 151-157.

[67] L. Graff, T. Crowe, M. Roberge, *Isolating the effect of material properties in the wear of soil engaging tools* The Canadian Society for Bioengineering (CSBE-SCGAB) and the American Society of Agricultural and Biological Engineers (ASABE), 2009 Annual Conference, Rodd's Brudenell River Resort, Prince Edward Island. 12-15 July 2009.

[68] S. A. Al-Suhaibani, A. E. Ghaly, *Effect of plowing depth of tillage and forward speed on the performance of a medium size chisel plow operating in a sandy soil* American Journal of Agricultural and Biological Sciences 5 (3) (2010) 247-255.

[69] M. Nalbant, A. T. Palali, *Effects of different material coatings on the wearing of plowshares in soil tillage* Turkish Journal for Agriculture 35 (2011) 215-223.

[70] A. Yazici, *Investigation of the reduction of mouldboard ploughshare wear through hot stamping and hardfacing processes* Turkish Journal for Agriculture 35 (2011) 461-468.

[71] ABAQUS 6.11-1-EF Documentation (ABAQUS/Explicit).